LEVEL III

ANNUAL TECHNICAL REPORT

1 October 1979 - 31 December 1980

ARPA Order:	3291-21
Program Code:	9D60
Contractor:	The Regents of the University of California University of California, San Diego La Jolla, California 92093
Effective Date:	1 October 1979
Expiration Date:	31 December 1980
Amount of Contract:	$110,000
Contract Number:	F49620-79-C-0019
Principal Investigators:	L. M. Dorman (714) 452-2406 J. A. Orcutt (714) 452-2887 T. H. Jordan (714) 452-2809
Program Manager:	Mr. William J Best
Title:	Seismic Detection and Discrimination Using Ocean-Bottom Seismographs
Sponsored by:	Advanced Research Projects Agency (DOD) ARPA Order No. 3291-21
Monitored by:	AFOSR under contract [redacted] F49620-79-C-0019

SECURITY CLASSIFICATION (When Data Entered) Unclassified

REPORT DOCUMENTATION PAGE

READ INSTRUCTIONS BEFORE COMPLETING FORM

1. REPORT NUMBER	2. GOVT ACCESSION NO.	3. RECIPIENT'S CATALOG NUMBER
AFOSR-TR-81-0535	AD-A101 082	

4. TITLE (and Subtitle)
Seismic Detection and Discrimination Using Ocean-Bottom Seismographs.

5. TYPE OF REPORT & PERIOD COVERED
Annual Technical Report
10/1/79 - 12/31/80

6. PERFORMING ORG. REPORT NUMBER
1 Oct 79-31 Dec 80

7. AUTHOR(s)
L. M. Dorman
J. A. Orcutt
T. H. Jordan

8. CONTRACT OR GRANT NUMBER(s)
F49620-79-C-0019
ARPA Order-3291

9. PERFORMING ORGANIZATION NAME AND ADDRESS
Regents of the University of California
University of California, San Diego
La Jolla, CA 92093

10. PROGRAM ELEMENT, PROJECT, TASK AREA & WORK UNIT NUMBERS
61101E
9D60 3291

11. CONTROLLING OFFICE NAME AND ADDRESS
Advanced Research Projects Agency/NMR
1400 Wilson Boulevard
Arlington, Virginia 22209

12. REPORT DATE
May 1981

13. NUMBER OF PAGES
73

14. MONITORING AGENCY NAME & ADDRESS *(if different from Controlling Office)*
Air Force Office of Scientific Research/NP
Bolling Air Force Base
Washington, DC 20332

15. SECURITY CLASS. *(of this report)*
unclassified

15a. DECLASSIFICATION/DOWNGRADING SCHEDULE

16. DISTRIBUTION STATEMENT *(of this Report)*
Approved for public release;
distribution unlimited.

17. DISTRIBUTION STATEMENT *(of the abstract entered in Block 20, if different from Report)*

18. SUPPLEMENTARY NOTES

19. KEY WORDS *(Continue on reverse side if necessary and identify by block number)*
Ocean bottom seismology, seismic noise, subduction zone.

20. ABSTRACT *(Continue on reverse side if necessary and identify by block number)*
Part I: Around January 29, 1980 a mild storm occurred on the Southern California coast. During this time one of our ocean bottom seismographs (O.B.S.) was periodically recording noise samples at 31°N, 119°48'W, about 370 km offshore in 4 km of water. We have compared the noise energy, as a function of time, recorded by the vertical seismometer with the following meteorological and oceanographic time sequences.
1. Wind speed at San Clemente, San Diego, Miramar and Los Angeles airports.
(over)

DD FORM 1 JAN 73 1473

UNCLASSIFIED
SECURITY CLASSIFICATION OF THIS PAGE (When Data Entered)

072380

Unclassified

2. Wave spectral density at La Jolla, Oceanside and Point Hueneme.
3. Surface weather maps.
4. Surface wind speed near the instrument as obtained from numerical weather modelling.

The noise energy in the 1-3 Hz frequency range correlates most strongly with the wave height on the nearby coast. The local and distant wind data were dissimilar in the durations of the disturbance and in the time of the peak amplitude.

We conclude that sea floor noise near 1 Hz comes predominantly from the surf. The nonlinear mechanisms which transfer energy from gravity waves on the sea surface into the sea floor are so inefficient at these frequencies that the contribution from surf a few hundred km away dominates the energy from the sea surface a few km away.

Part II: An array of 4 ocean-bottom seismometers (O.B.S.) was operated for one month during June-July, 1977 at 16.5°N, 100.5°W in the Middle America Trench near Acapulco. The purpose of the experiment was to investigate the seismicity of the accretionary prism and to study the propagation of seismic waves across the continental margin. The location of earthquakes occurring landward of the OBS array was controlled by a 7-station land-based array operated by a team of Mexican seismologists under the direction of Dr. Lautaro Ponce Mori. Two patterns in the spatial distribution of seismicity were detected. The majority of the epicenters were more-or-less uniformly distributed landward of a line lying approximately 20 km offshore and parallel to the coastline, roughly coinciding with the magnetically-determined edge of continental crust (Karig et al., 1978). Hypocenters for these events were located both within the descending slab and above it. Activity more than 20 km offshore was restricted to a salient of seismicity perpendicular to the trench on a line coincident with a right-lateral offset of the 1000-m isobath. Hypocenters in this salient were located within the descending slab and appear to be indicative of scissor faulting of a segmented plate. No seismicity was associated with the accretionary prism.

PART I

Preliminary Results of the LINER Experiment:

Correlation of Sea Floor Noise and Meteorology and Causality

LeRoy M. Dorman

Chin-Yen Huang

Abstract

Around January 29, 1980 a mild storm occurred on the Southern California coast. During this time one of our ocean bottom seismographs (O.B.S.) was periodically recording noise samples at 31°N, 119°48'W, about 370 km offshore in 4 km of water. We have compared the noise energy, as a function of time, recorded by the vertical seismometer with the following meteorological and oceanographic time sequences.

1. Wind speed at San Clemente, San Diego, Miramar and Los Angeles airports.
2. Wave spectral density at La Jolla, Oceanside and Point Hueneme.
3. Surface weather maps.
4. Surface wind speed near the instrument as obtained from numerical weather modelling.

The noise energy in the 1-3 Hz frequency range correlates most strongly with the wave height on the nearby coast. The local and distant wind data were dissimilar in the durations of the disturbance and in the time of the peak amplitude.

We conclude that sea floor noise near 1 Hz comes predominantly from the surf. The nonlinear mechanisms which transfer energy from gravity waves on the sea surface into the sea floor are so inefficient at these frequencies that the contribution from surf a few hundred km away dominates the energy from the sea surface a few km away.

Introduction

The background noise observed on the sea floor undoubtedly contains contributions from many sources, and the relative importance of each varies with time, location and frequency. Among the likely candidates we can

number 1) waves on the sea surface, 2) ocean waves breaking on shores, 3) ocean currents impinging on the measuring instrument, 4) internal waves in the water, 5) natural biological activity and 5) cultural or "human" noise.

During the time period December 1979 - February 1980 we undertook a modest ocean-bottom noise experiment called LINER, so named because of its proximity to the line between U.S. and Mexican territorial waters. Because we thought at the time that tidal currents were likely to be contributors, we chose a site previously used for tidal studies by Munk, Snodgrass and Wimbush (1980). The site was named JOSIE 175 and is about 375 km off the California coast (see Figure 1). The treatment we present here is an extended version of that given by Huang and Dorman (1980).

Observations

Observations of vertical ground motion were made using the ocean bottom seismograph designed by Prothero (1976). These instruments use a 1 Hz vertical seismometer as a sensor and feature programmed or triggered recording. The data are digitized with 12-bit accuracy and recorded in serial form on ¼-inch magnetic tape. Recording capacity is 3 hours and 20 minutes at a sampling rate of 128 per second. The signal is digitized continuously, even when the recorder is not running. This digitized data immediately enters a digital delay line with a length of 12 seconds. Thus, when the recorder starts it begins recording data from 12 seconds into the past. By this means we obtain a sample of data taken while the mechanical tape recorder is not running and thus is free from disturbance.

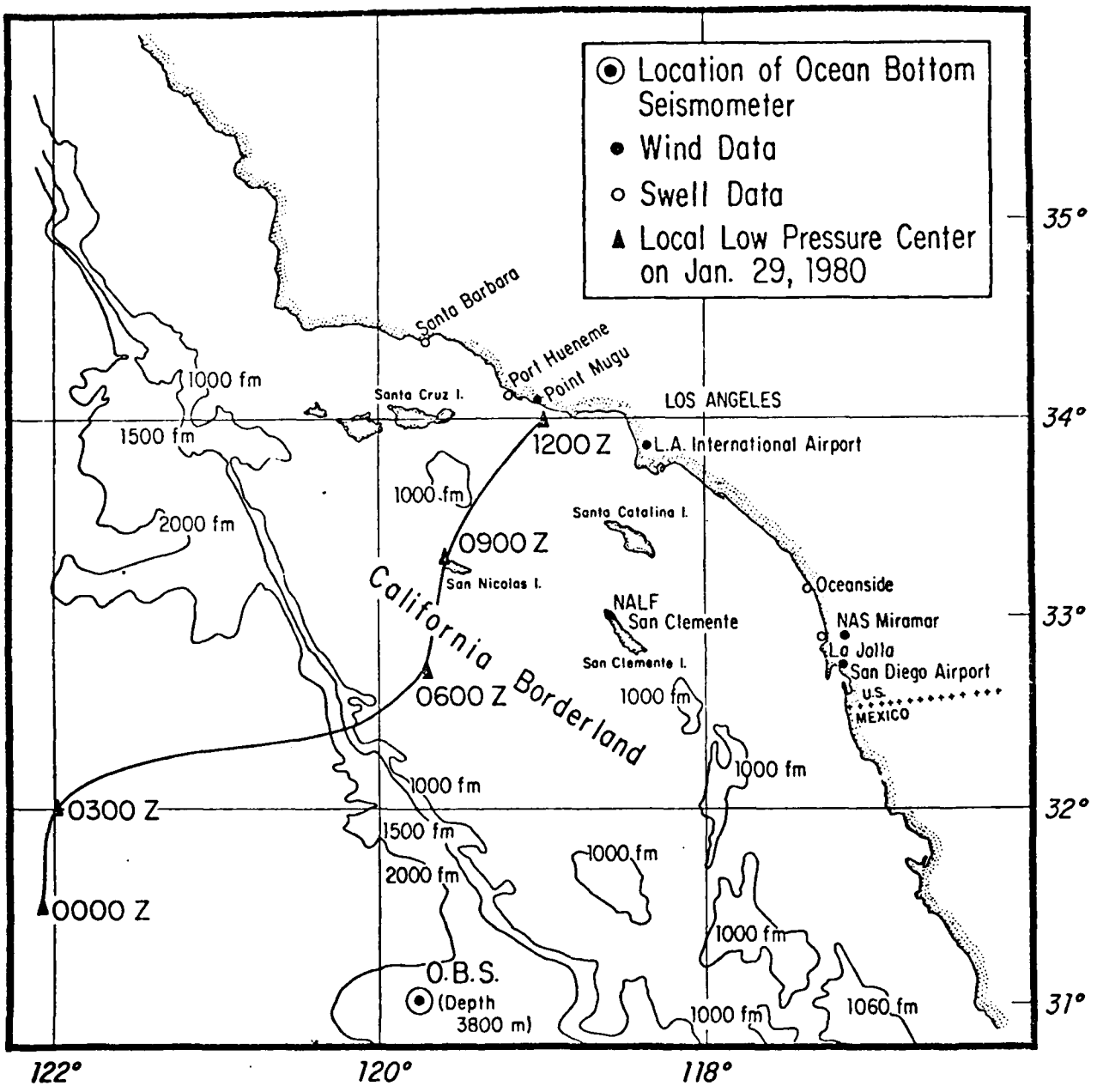

Figure 1. Location chart for the LINER experiment. The large variations in storm velocity along the track and the sinuosity of the track probably represent measurement errors rather than real irregularities in the storm's course and speed.

The current meters we deployed showed that the maximum tidal current was less than 4 cm s^{-1}. Figure 2 shows spectral averages of background noise in four spectral bands from 1/8 Hz to 16 Hz. We see that there are no sensible indications of diurnal or semi-diurnal periodicities.

During the course of the experiment a mild meteorological depression passed to the northwest of the instrument site and dissipated when it encountered the coast. This low pressure center, with its accompanying winds, caused a distinctive signature in the seafloor noise, windspeed and surf height and allowed us to identify the influence of this storm. The storm track, measured from the 3-hourly maps of the National Weather Service is shown in Figure 1. The sinuosity of the track and the radical variations in the velocity along the track are probably due to imprecision in the storm center locations.

The instrument was located at a site remote from shipping lanes and other sources of meteorological data so we obtained an estimate of surface conditions from the numerical model of the Fleet Numerical Weather Center at Monterey, California. This estimate of surface pressure is shown at the top of Figure 3, along with measurements at other locations referred to in Figure 1. They clearly show the same form, except the model record is smoother than the observations at the various observatories.

Figure 4 shows the surface wind from the numerical model compared with land observations. We note that they are grossly similar in shape with the exception that the wind at the instrument site leads the land observations by about 12 hours.

The surface wind field was that for the closest grid point (30°N,119°W) of the Fleet Numerical Weather Center surface analysis. This uses the

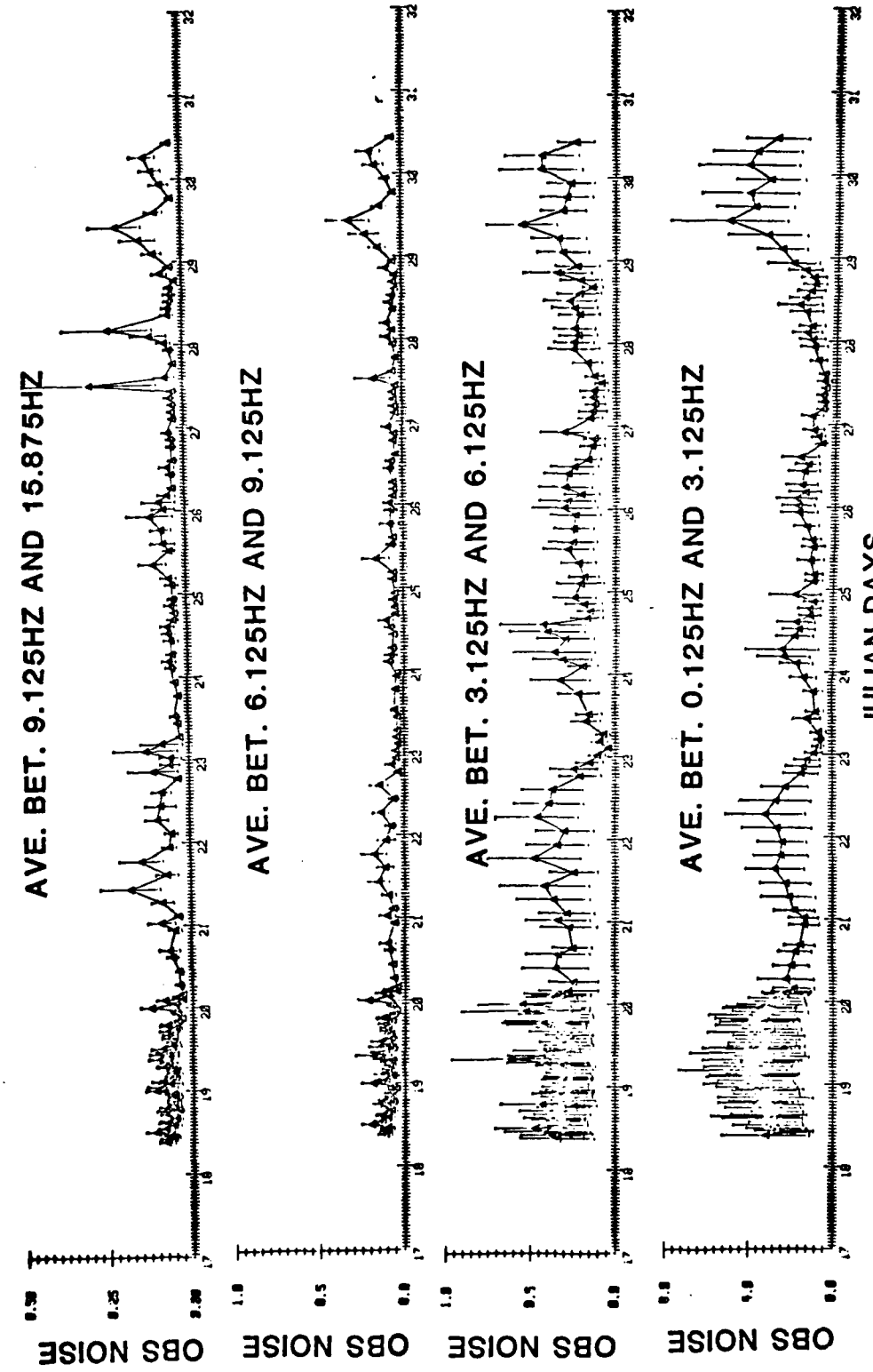

Figure 2. Spectra in four frequency bands for a twelve-day period. No tidal periodicities are obvious.

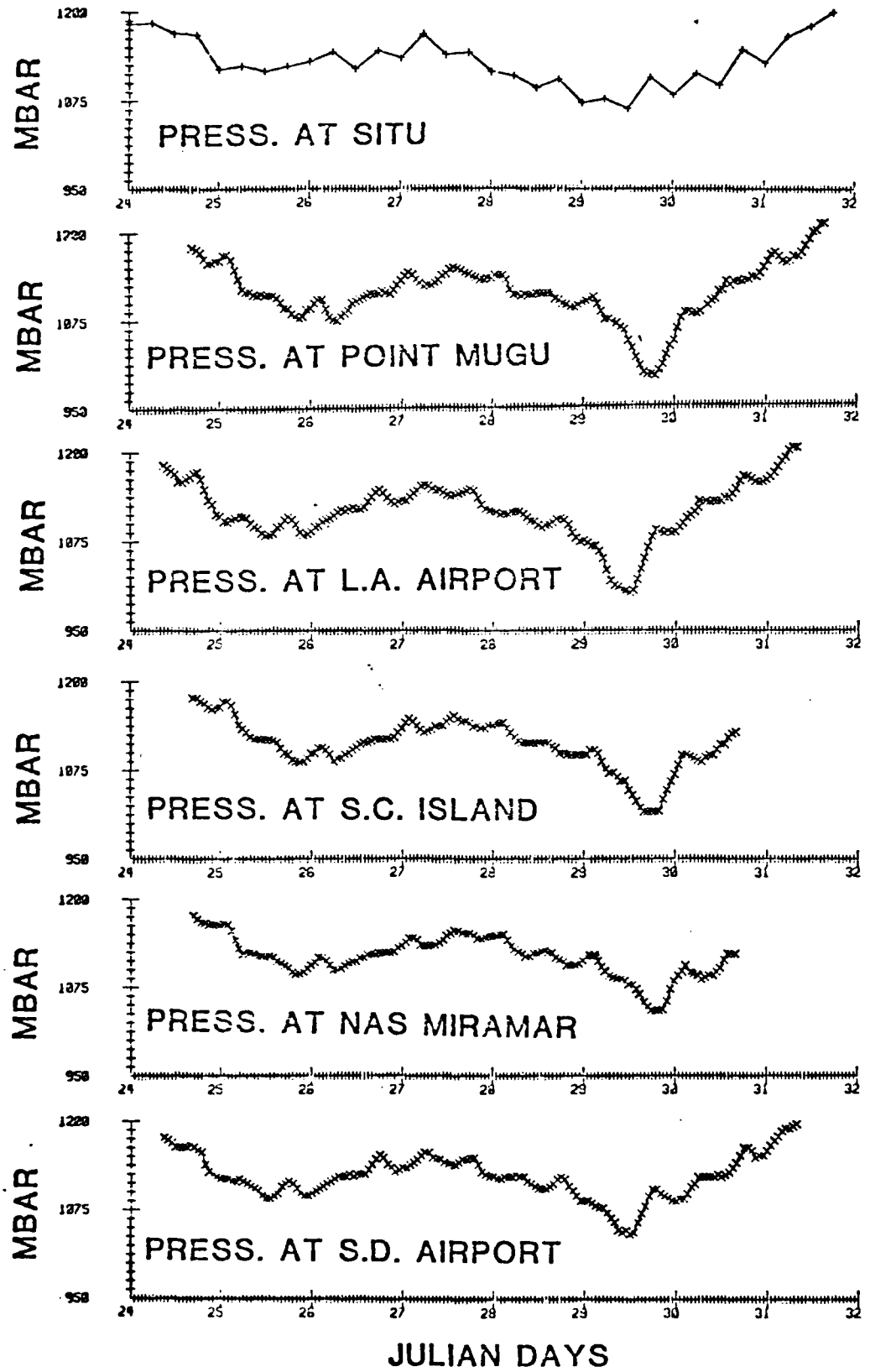

Figure 3. Surface air pressure from the numerical weather model (top) along with actual observations at nearby land station.

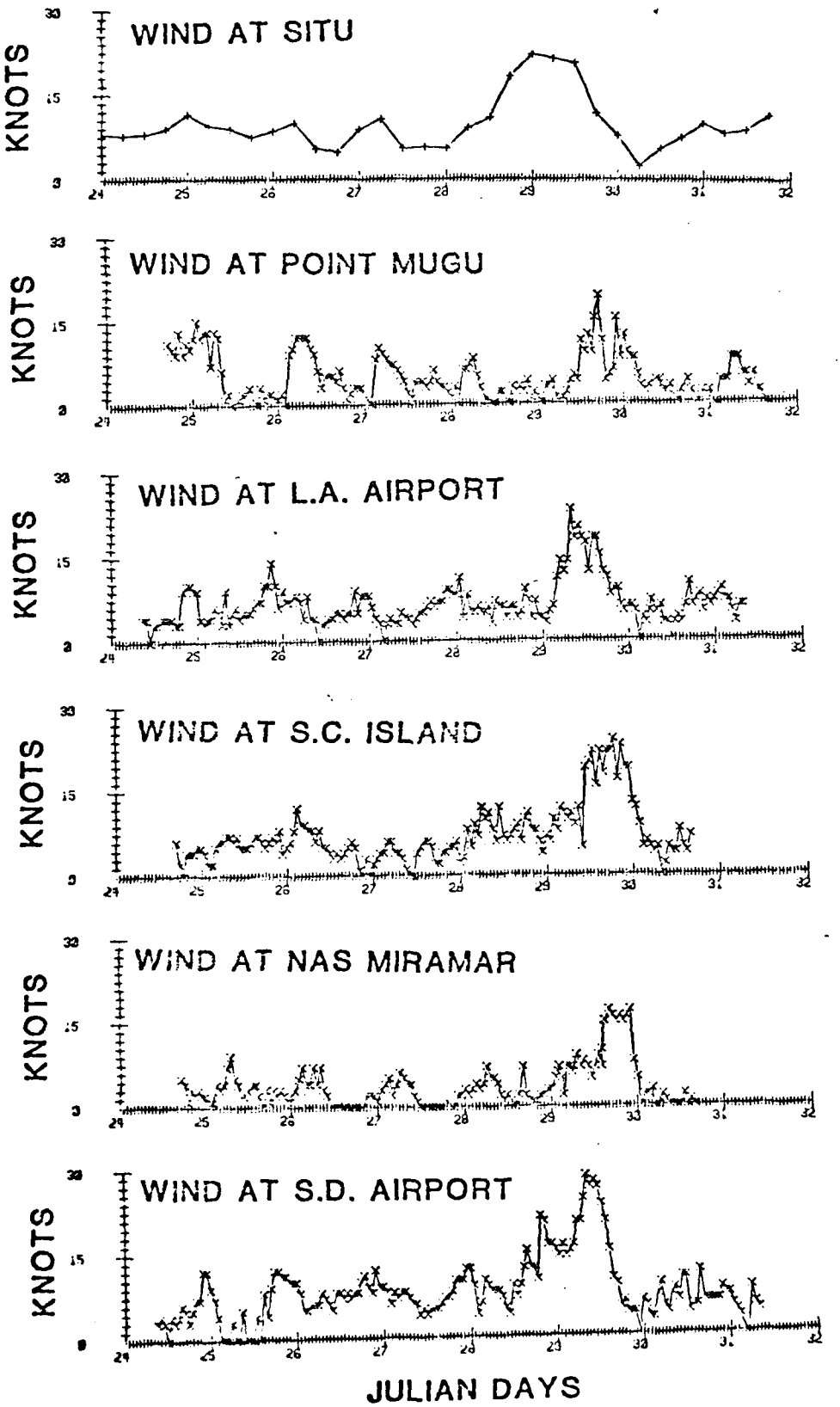

Figure 4. Surface wind speeds from the numerical model (top) and observations at nearby land stations.

FIB (Fields by Information Blending) methodology (see Caton et al., 1978) based on present and past observations only. It thus must be causal. (If hindcasting were used, we could not make our argument based on the observation that the surface wind leads to seismic noise in time.)

In addition to the weather data, we examined observations of surf conditions on the California coast. The California Resources Agency Department of Boating and Waterways supports the California Coastal Engineering Network, operated by R. Seymour of SIO's Institute for Marine Resources, to monitor oceanographic conditions which affect boating and the engineering of coastal structures. This network consists of sea floor pressure sensors and waverider buoys, operated singly and in arrays. The data are digitally telemetered to SIO and recorded. Figure 5 shows total swell "power" at four locations indicated on Figure 1. We note that the onset of the swell associated with the storm of day 29 occurs simultaneously at all stations to the accuracy permitted by the 6-hour sampling interval.

Figures 6 and 7 show wind and swell on the coast along with the wind at the instrument site and the observed background noise. Very clearly, the noise is most highly correlated with the wind and swell at the coast. The wind at the instrument site leads the OBS noise by about half a day, and thus cannot be the proximate cause of the noise.

Figure 8 is a similar presentation except that higher frequency background noise is shown. The correlation is much less pronounced, indicating that coastal swell conditions control the background noise in the .125-3 Hz band but do not greatly affect the 3-16 Hz band.

Figure 9 shows power spectra of ground accelejation during 3 time periods. The spectrum marked "noisy period" was calculated using data

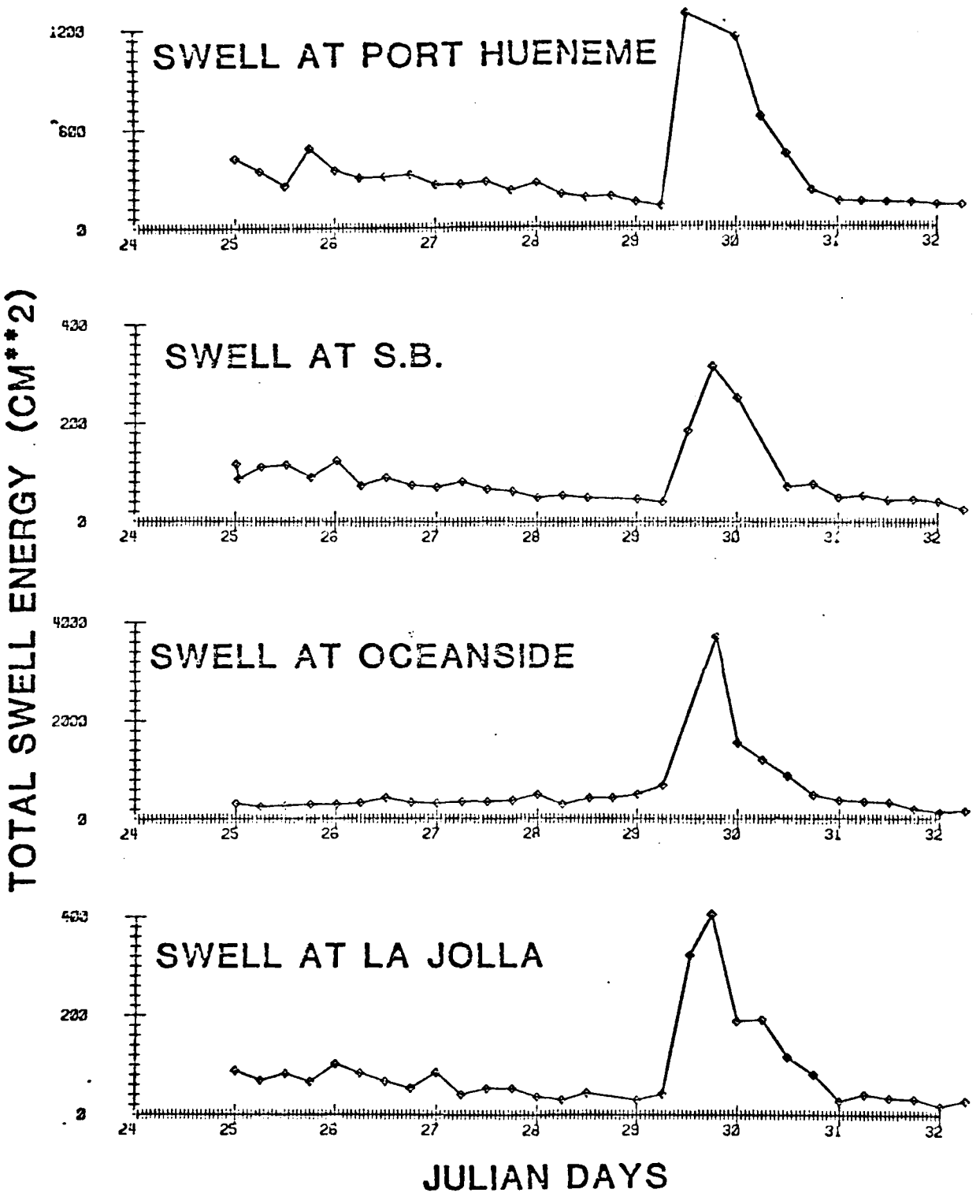

Figure 5. Swell power at several stations in the California Coastal Engineering Network for a time period including the storm.

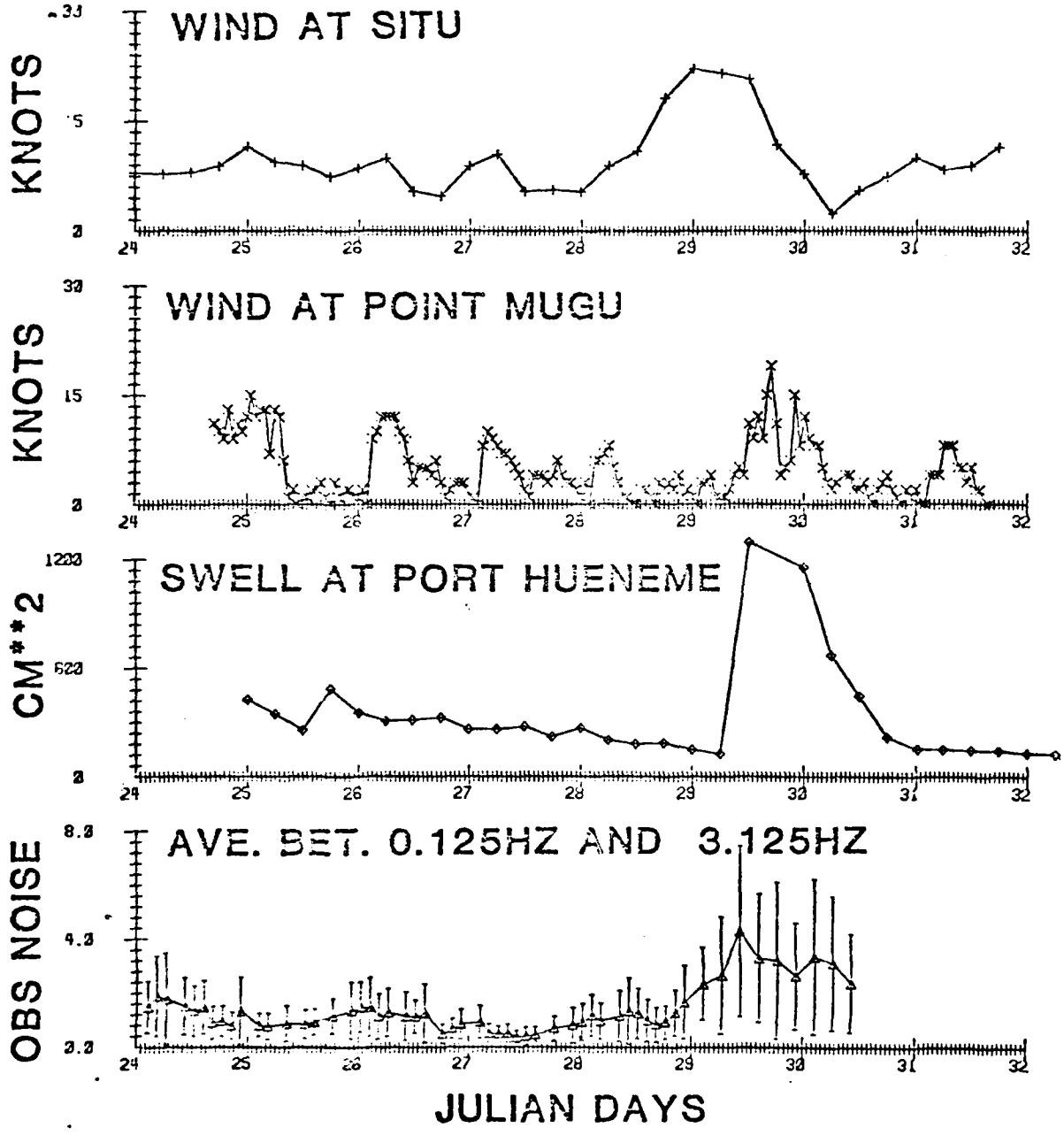

Figure 6. Wind, swell and sea floor noise in the .125 - 3.125 Hz band.

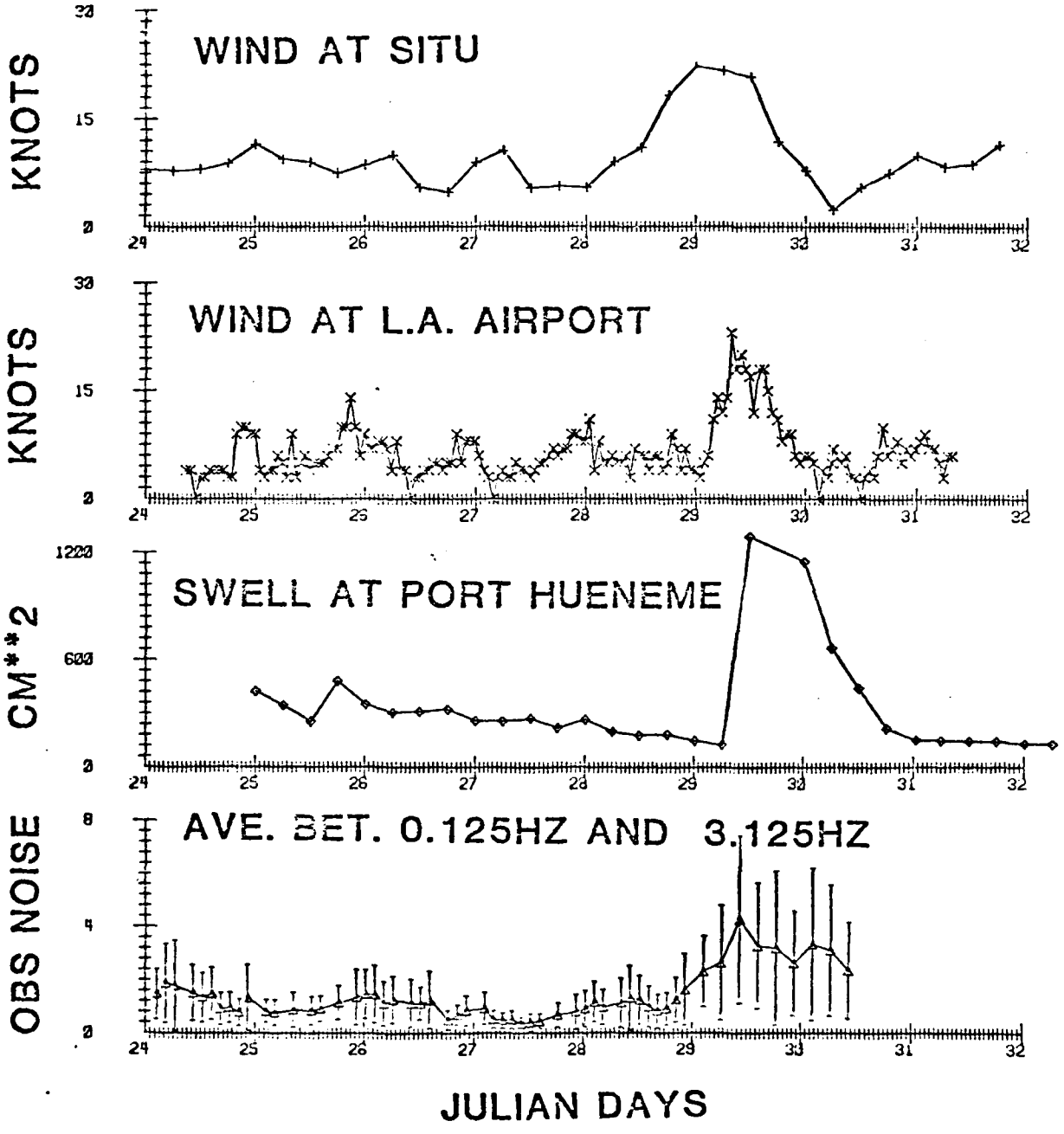

Figure 7. Wind, swell and sea floor noise in the .125 - 3.125 Hz band.

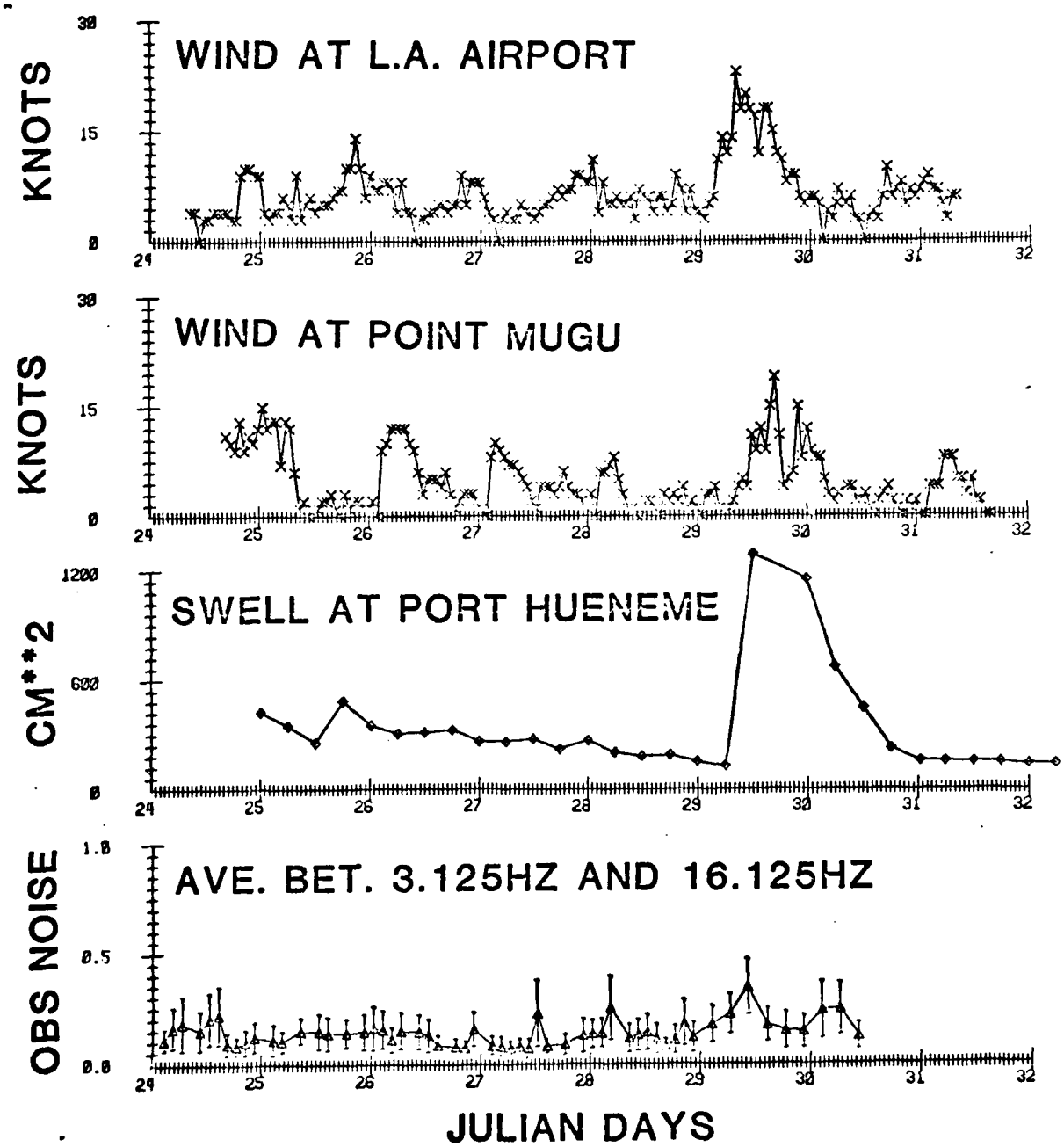

Figure 8. Wind, swell and sea floor noise in the 3.125 - 16.125 Hz band.

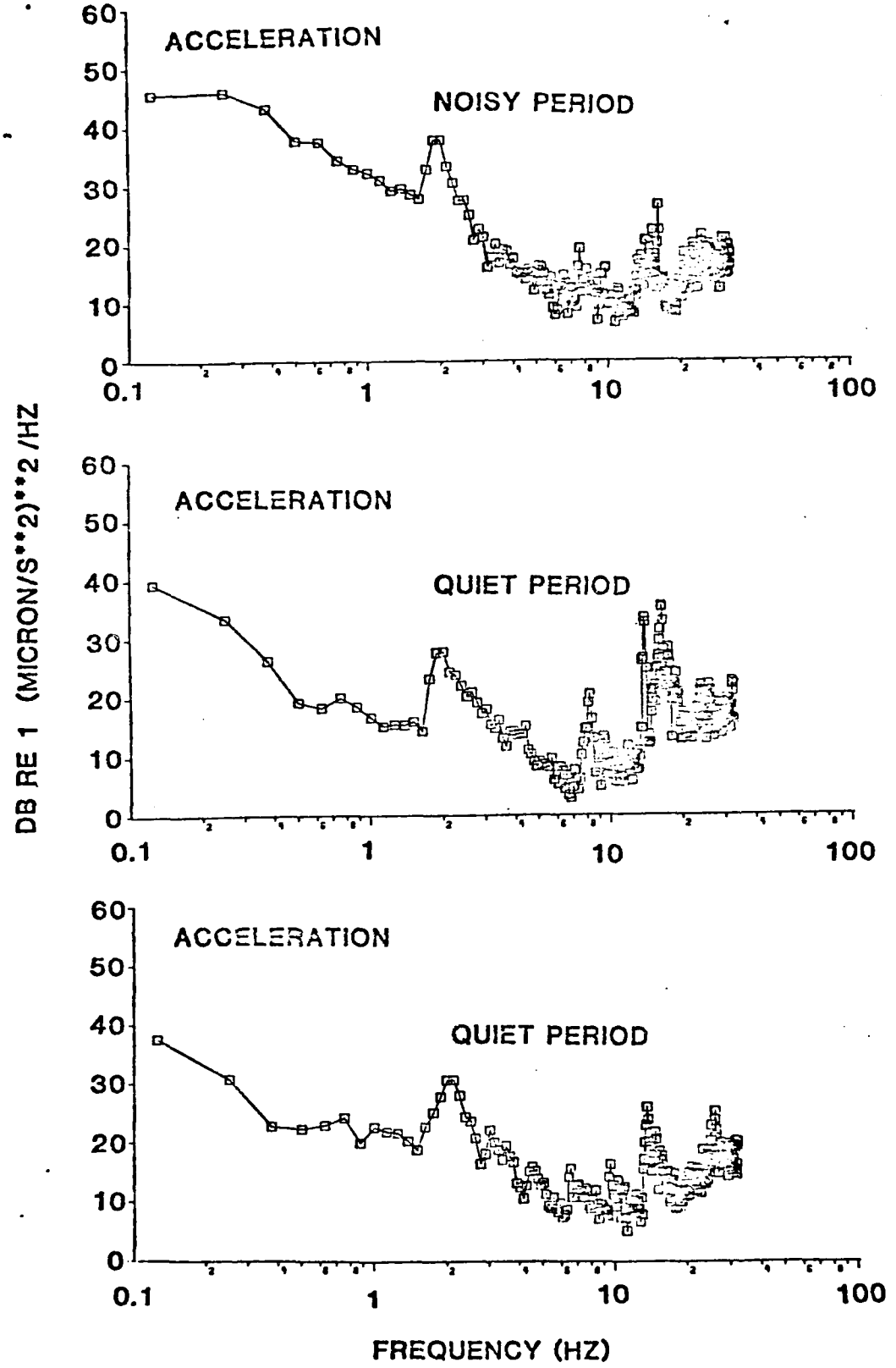

Figure 9. Power spectra in ground motion for quiet and noisy time periods. We have plotted acceleration instead of amplitude since the earth noise is, on the average, flat in acceleration over many decades. Plotting acceleration preserves more detail in the presentation in the same manner as a reduced travel time plot.

from the time of high background noise and swell. The two spectra marked "quiet period" characterize non-stormy conditions. Several things are evident from these spectra:

1) The storm has affected mainly the 0.2-3.0 Hz band, leaving the higher frequencies largely unaffected.

2) In the 0.2 - 3.0 Hz band, the level has been raised by about 10 dB, while leaving the fine structure - specifically the peak at 2. Hz - unaltered. This indicates that mechanisms generating the background noise during the quiet period are probably the same as those which are dominant during the noisy period. If the mechanisms were different we would expect to see an additive change rather than a multiplicative one.

Haubrich and McCamy (1969) in their benchmark study of the wavenumber-frequency characteristics of vertical microseismic noise observed at LASA (on land) described their salient properties. They are that:

1. The ≈70 mHz (14 s) microseism band derive most of their energy from ocean waves impinging on coasts. These propagate predominantly as Rayleigh waves.
2. The ≈140 mHz (7 s) microseism band contains both body wave and surface wave energy. The body waves appear to be generated by fast-moving storms which can set up the interference pattern required for the Longuet-Higgins (1950) mechanism. The surface waves in this band come from coastal areas, as in the 70 mHz band.
3. Body waves are dominant above 200 mHz (5 s). They appear to have the same source characteristics as the 140 mHz noise.

From the causality argument made earlier, we can associated the 0.125 - 3.125 Hz noise with surf breaking. Since we had only a single

component vertical instrument operating we can make no definitive statements about the propagation mechanism. Experience with sea floor noise at other locations, however, is that the sea floor noise has low correlation length and hence short wavelength. This implies high wavenumber propagation such as is characteristic of waveguides. The observations of Okal and Talandier (in press) of efficient propagation of 1 Hz Rayleigh waves propagating in the sedimentary waveguide indicate that this waveguide is certainly effective in energy transport.

Conclusions

Tidal currents at the recording site were low, less than 4 cm/s, and did not contribute significantly to the seismic noise recorded on the vertical component instrument; there were no sensible indications of diurnal or semi-diurnal periodicities in the noise amplitude. Correlations with wind and surf observations along the Southern California coast suggest that, in the frequency band 0.2 - 3.0 Hz, the dominant noise source is surf-excited disturbances propagating from the coast as surface, interface or wave-guide modes.

References

Caton, Francis G., M. G. Caming and B. R. Mendenhall, 1978. A northern hemisphere history of wind-based parameters, Technical Repot MIT project M-231 (Contract no. 03-78-M02-126, PEG, NOAA, NMFS, Meteorology international, Incorporated, Monterey, California, 116 pp.).

Haubrich, R.A. and K. McCamy, 1969. Earth noise, coastal and Pelagic sources, J. Geophys. Res, *

Huang, C.-Y. and L. M. Dorman, 1980. Correlation of sea floor noise and meteorology, EOS, Trans., AGU, 61, 1047-1048.

Munk, W., F. Snodgrass and M. Wimbush, 1970. Tides off-shore transition from California coast to deep-sea waters, Geophys. Fluid Dynamics, 1, 161-235.

Okal, E. D. and J. Talandier, 1980. Dispersion at one-second Rayleigh modes through oceanic sediments following shallow earthquakes in the south-central Pacific Ocean Basin, Proc. of the SACLANT-ASW Conference on Bottom Interacting Ocean Acoustics, La Speria (in press).

Prothero, W.A., 1976. A free fall seismic capsule for seismicity and refraction work, Offshore Technology Conference, Paper No. 2440.

PART II

Ocean-Bottom and Land-Based Seismograph Study of the Middle America Trench near 16.5°N, 100.5°W

Keith A. Sverdrup
Thomas H. Jordan

ABSTRACT

An array of 4 ocean-bottom seismometers (OBS's) was operated for one month during June-July, 1977 at 16.5°N,100.5°W in the Middle America Trench near Acapulco. The purpose of the experiment was to investigate the seismicity of the accretionary prism and to study the propagation of seismic waves across the continental margin. The location of earthquakes occurring landward of the OBS array was controlled by a 7-station land-based array operated by a team of Mexican seismologists under the direction of Dr. Lautaro Ponce Mori. Two patterns in the spatial distribution of seismicity were detected. The majority of the epicenters were more-or-less uniformly distributed landward of a line lying approximately 20 km offshore and parallel to the coastline, roughly coinciding with the magnetically-determined edge of continental crust (Karig et al., 1978). Hypocenters for these events were located both within the descending slab and above it. Activity more than 20 km offshore was restricted to a salient of seismicity perpendicular to the trench on a line coincident with a right-lateral offset of the 1000-m isobath. Hypocenters in this salient were located within the descending slab and appear to be indicative of scissor faulting of a segmented plate. No seismicity was associated with the accretionary prism.

INTRODUCTION

In June, 1977 Scripps conducted a seismicity survey of the Middle America Trench and adjacent continental margin in cooperation with the Universidad Nacional Antonoma de Mexico approximately 50 km northwest of Acapulco (Figure 1).

Scripps deployed four OBS's in an array centered at about 16.5°N, 100.5°W. Two capsules, Gwen and Inez, were located in the axis of the trench while the remaining two, Deni and Doe, were on the inner wall of the trench. The spacing between capsules was about 15 km.

A team of Mexican seismologists under the direction of Dr. Lautaro Ponce Mori operated a seven-element land-based array 75 km from the OBS's. Each element of the land array consisted of a vertical-component analog-recording seismograph. The distance between instruments ranged from about 6 to 18 km.

The purpose of this experiment was to investigate in detail the seismicity located in the vicinity of the trench and the continental margin. The questions we wished to address were: Is the accretionary prism seismically active?, and, What is the relationship of the spatial distribution of the seismicity to the subducting oceanic plate and the overriding continental plate?

TECTONIC SETTING

The Middle America Trench extends for 2600 km marking the line of subduction of the Cocos Plate beneath southern Mexico and

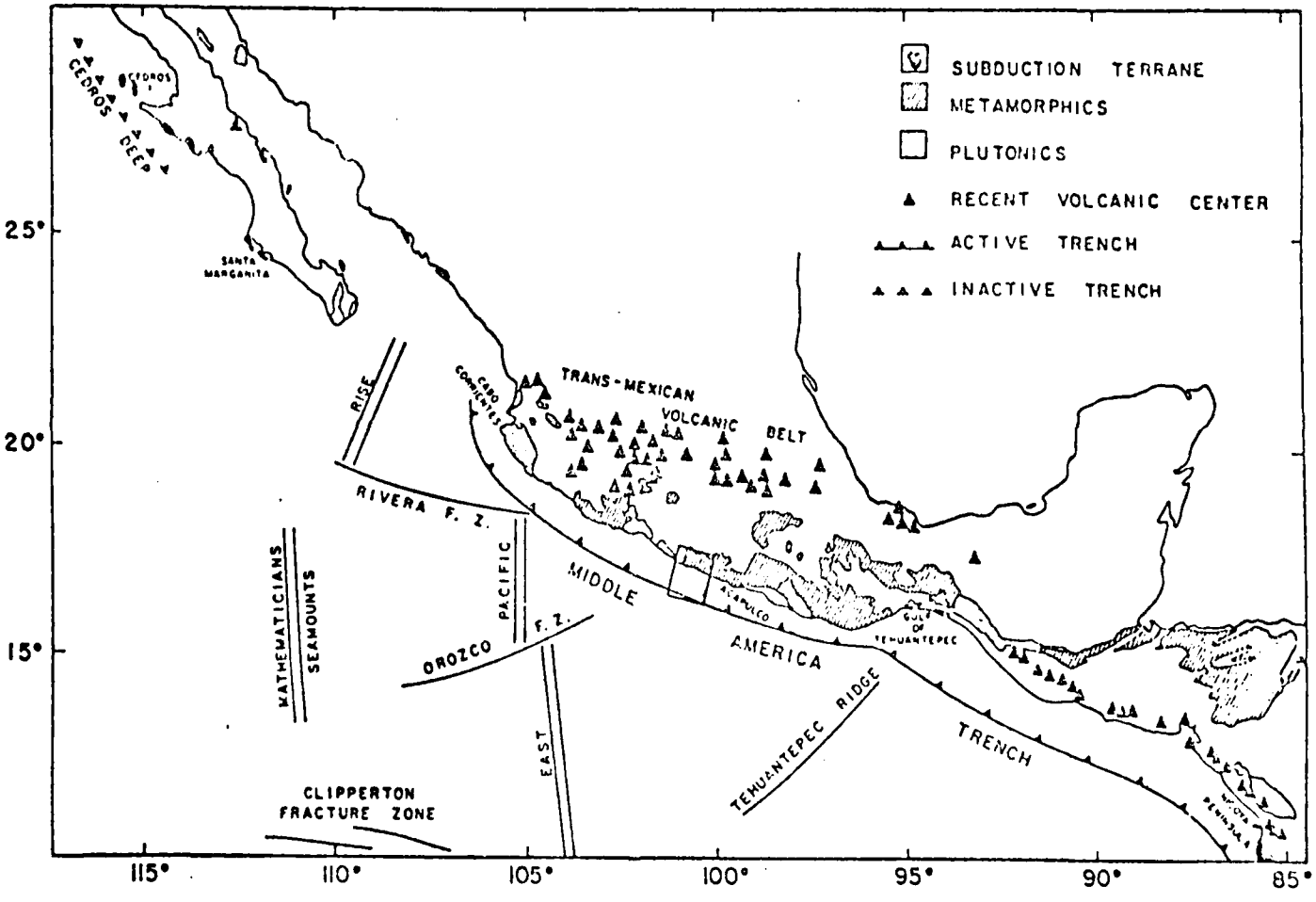

Figure 1. Map of northern Middle America Trench region after Karig et al. (1978) showing plate boundaries and geologic features. Box indicates location of survey area.

Central America. The general morphology and structure of the trench and continental margin have been discussed in detail by Fisher (1961), Shor and Fisher (1961), and Ross and Shor (1965) among others.

A fundamental change in the morphology of the continental margin occurs at the Gulf of Tehuantepec where the Tehuantepec Ridge intersects the trench. The continental shelf is narrow to the northwest and widens to the southeast (Shor, 1974; Seeley et al., 1974). Karig et al. (1978) have suggested that the narrow shelf off the coast of Mexico is the result of right-lateral oblique subduction prior to late Miocene time that tectonically eroded the continental margin.

The Gulf of Tehuantepec also marks a distinct change in the spatial distribution of active volcanism on land. To the southeast the volcanoes of Central America form lineaments parallel to the trench within 50 km of the coast (Stoiber and Carr, 1973). In contrast the active volcanoes of southern Mexico are spatially diffuse, occurring in a wide belt that trends roughly east-west at an angle to the strike of the trench (Mooser, 1973).

The teleseismically located seismicity associated with the subduction of the Cocos plate is concentrated in a belt roughly 250 km wide extending the length of the trench (Figure 2). The complex spatial distribution of the seismicity with depth is evident in Figure 3 where the seismicity is plotted in cross section projected onto a plane parallel to the trench. Events are restricted to depths of 150 km or less northwest of the Gulf of Tehuantepec while to the

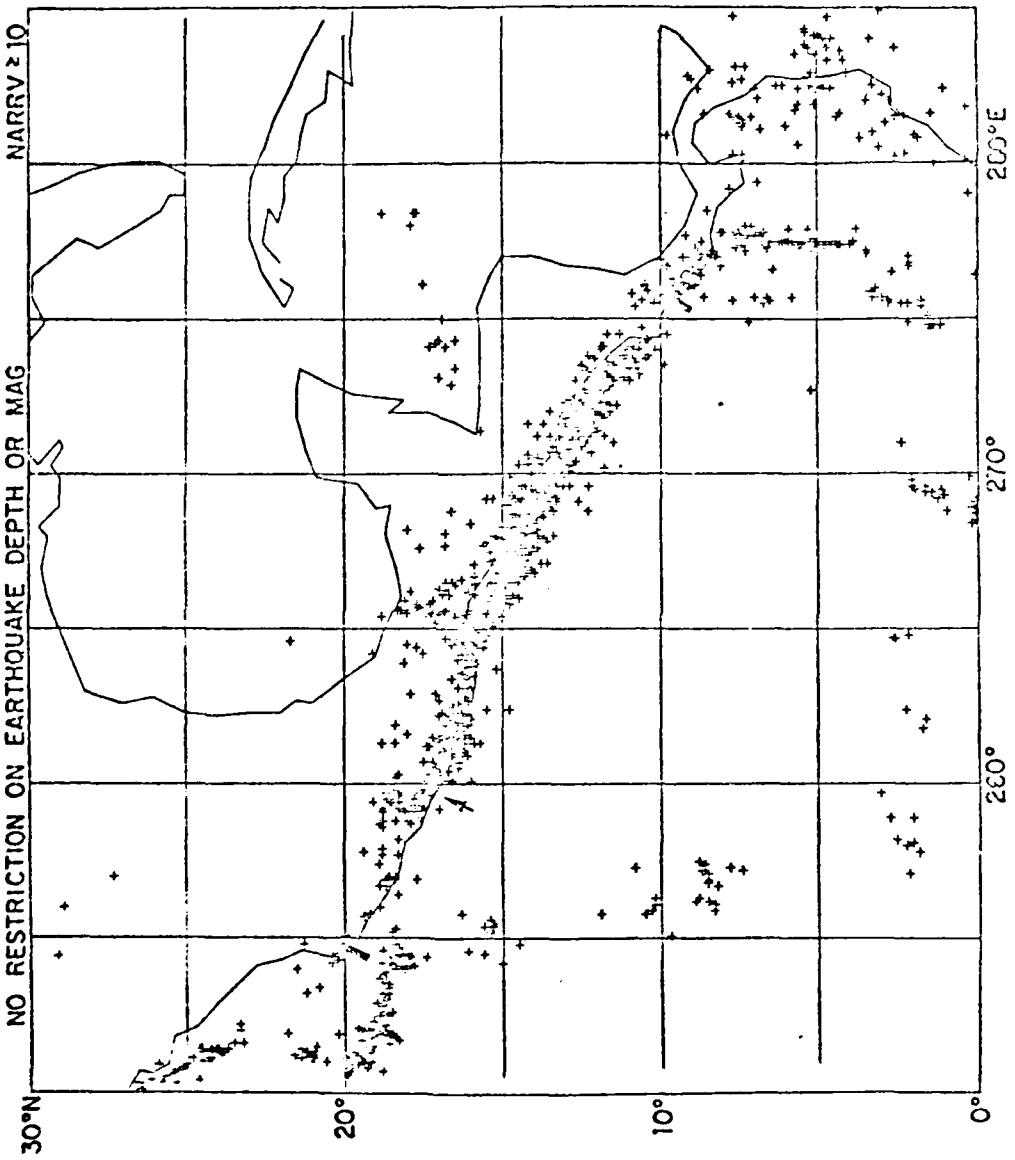

Figure 2. Plot of the seismicity recorded by ten or more stations in the time period 1965 to 1977 without regard to event depth or magnitude. Location of the survey area indicated by the arrow.

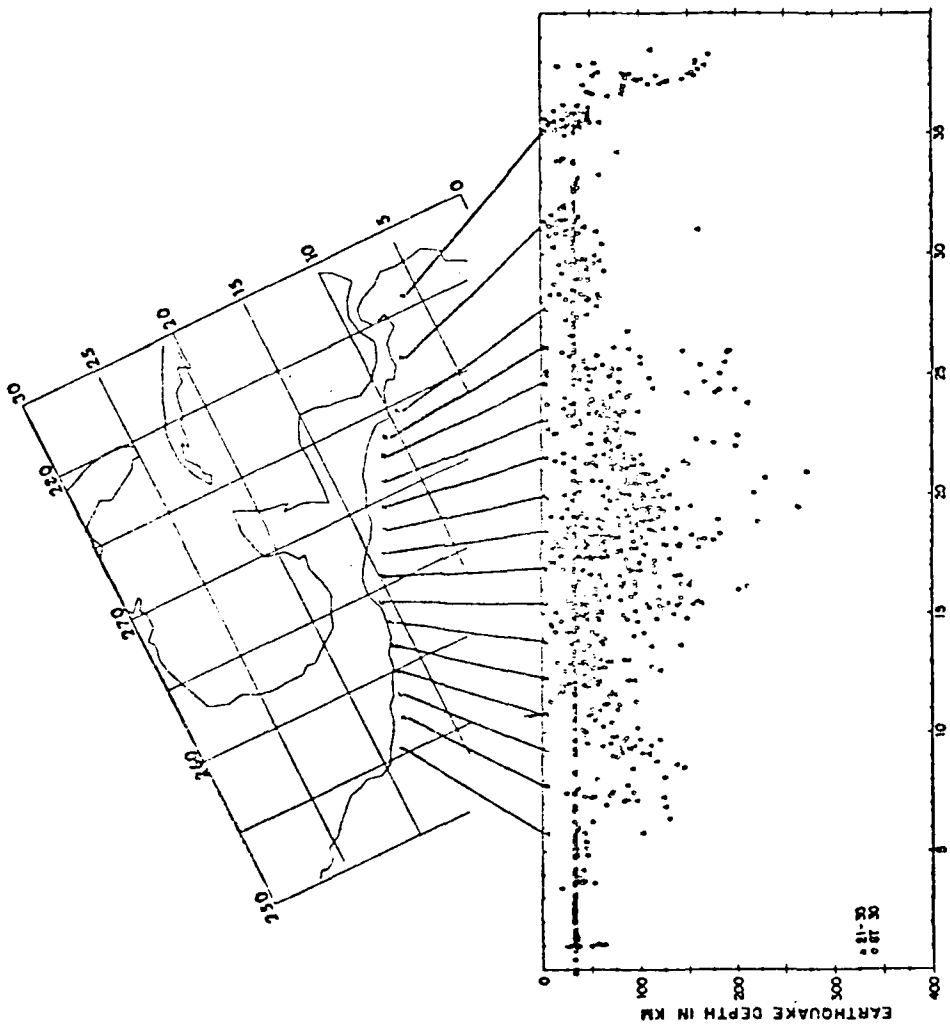

Figure 3. Hypocenters of events recorded by 21-30 stations (triangles) and more than 30 stations (circles) projected onto a plane parallel to the trench. Location of the survey area indicated by the arrow.

southeast earthquakes occur at depths of nearly 300 km in some areas. This difference is due to the shallower dip of the Benioff zone beneath Mexico with respect to Central America. Dean and Drake (1978) report that focal mechanisms of 28 shallow focus events caused by underthrusting of the Cocos Plate have slip vectors whose mean plunge increases from 15° for events located along the coast of Mexico to 21° for events along the coast of Central America. Contours of the depth of the Benioff zone show a strong correlation between the locations of active volcanoes on land and the surface projection of the 150 km depth contour in Central America and its extrapolated position across Mexico (Figure 4).

On a finer scale Stoiber and Carr (1973) have proposed that the subducted plate is divided into 100 to 300 km wide segments that have different strikes and dips. The location of segment boundaries along the Middle America arc have been inferred by offsets in the linear volcanic chains of Central America, the transverse alignment of cinder cones in southern Mexico, and strike-slip earthquake focal mechanisms at intervals along the arc characterized by one steeply dipping nodal plane which strikes roughly perpendicular to the trench (Stoiber and Carr, 1973; Carr et al., 1974; Carr and Stoiber, 1977; Dean and Drake, 1978). The locations of proposed boundaries between individual segments in southern Mexico are shown in Figure 5. The solid dot in the trench at the end of one of the proposed boundaries marks the location of the OBS array deployed during this experiment.

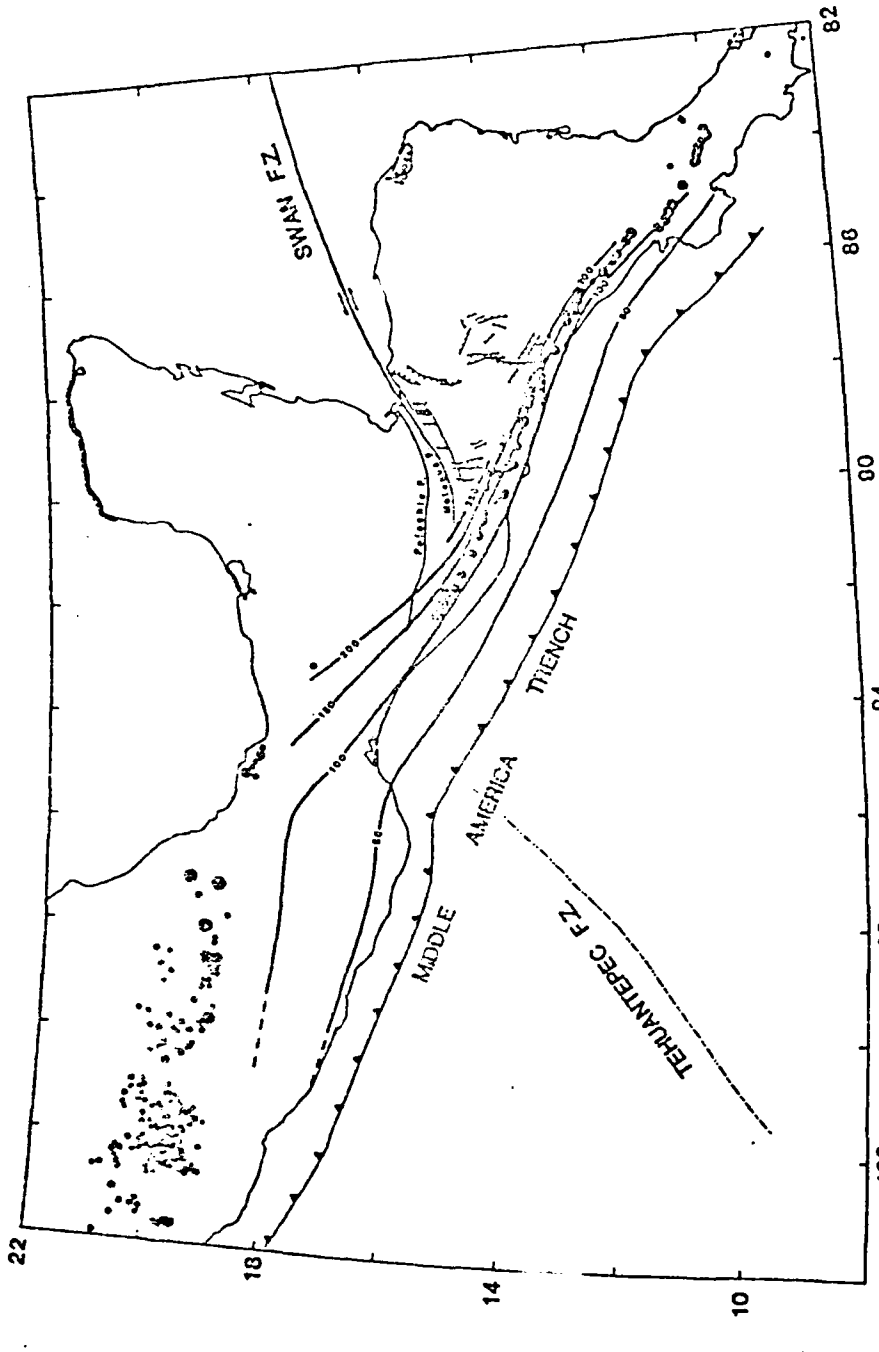

Figure 4. Depth to the Benioff zone contoured at 50 km intervals. Location of active volcanoes and cinder cones indicated by solid dots.

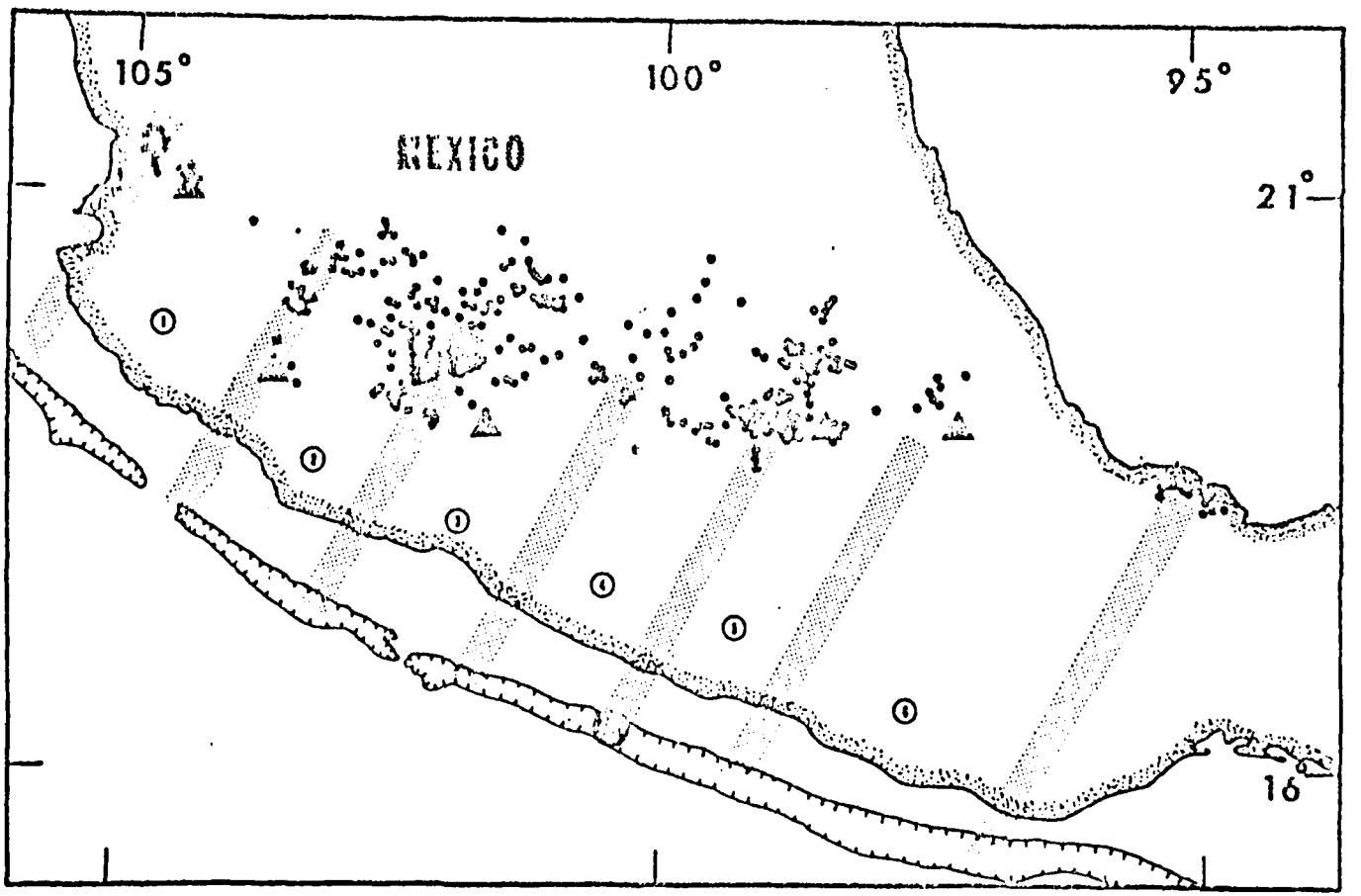

Figure 5. Volcanic segments of Mexico. Solid triangles represent historically active volcanoes (Mooser et al., 1958). Small circles are cinder cones (de Cserna, 1961). Stippled bars represent proposed boundary areas (Stoiber and Carr, 1973). Solid dot in trench axis marks OBS drop site.

The segmentation of subducted plates in various subduction zones has been discussed by numerous authors. Carr et al. (1973) concluded that the subducted plate beneath the Japanese islands is divided into sections based on abrupt changes in the strike and dip of the Benioff zone. Stauder (1968, 1972) suggested that the Aleutian Islands behave as independent blocks from the observation of aftershock regions of large earthquakes. Changes in the geometry of the Benioff zone beneath Chile were used by Swift and Carr (1974) to identify individual segments of the subducted plate. In addition focal mechanism studies have provided evidence supporting the segmentation of the oceanic plate along the Kurile-Kamchatka arc (Veith, 1974) and Indonesian arc (Fitch, 1970). Therefore, the segmentation of the Cocos Plate along the Middle America arc is not unique.

A detailed marine geophysical study was conducted by Karig et al. (1978) in the immediate vicinity of the survey area. Figure 6 is a bathymetric map of the area contoured in meters, corrected with Mathew's tables. Karig et al. (1973) were able to identify seafloor magnetic anomalies up to 30 km landward of the trench extending beneath the inner trench slope. Estimates of the depth of the oceanic crust based on the intensity of the anomalies suggest that the subducting plate dips roughly 8° beneath the accretionary prism. Magnetic anomalies associated with the continental metamorphic basement could be traced 20 to 30 km offshore. The contact between the oceanic and continental anomalies is very regular and nearly

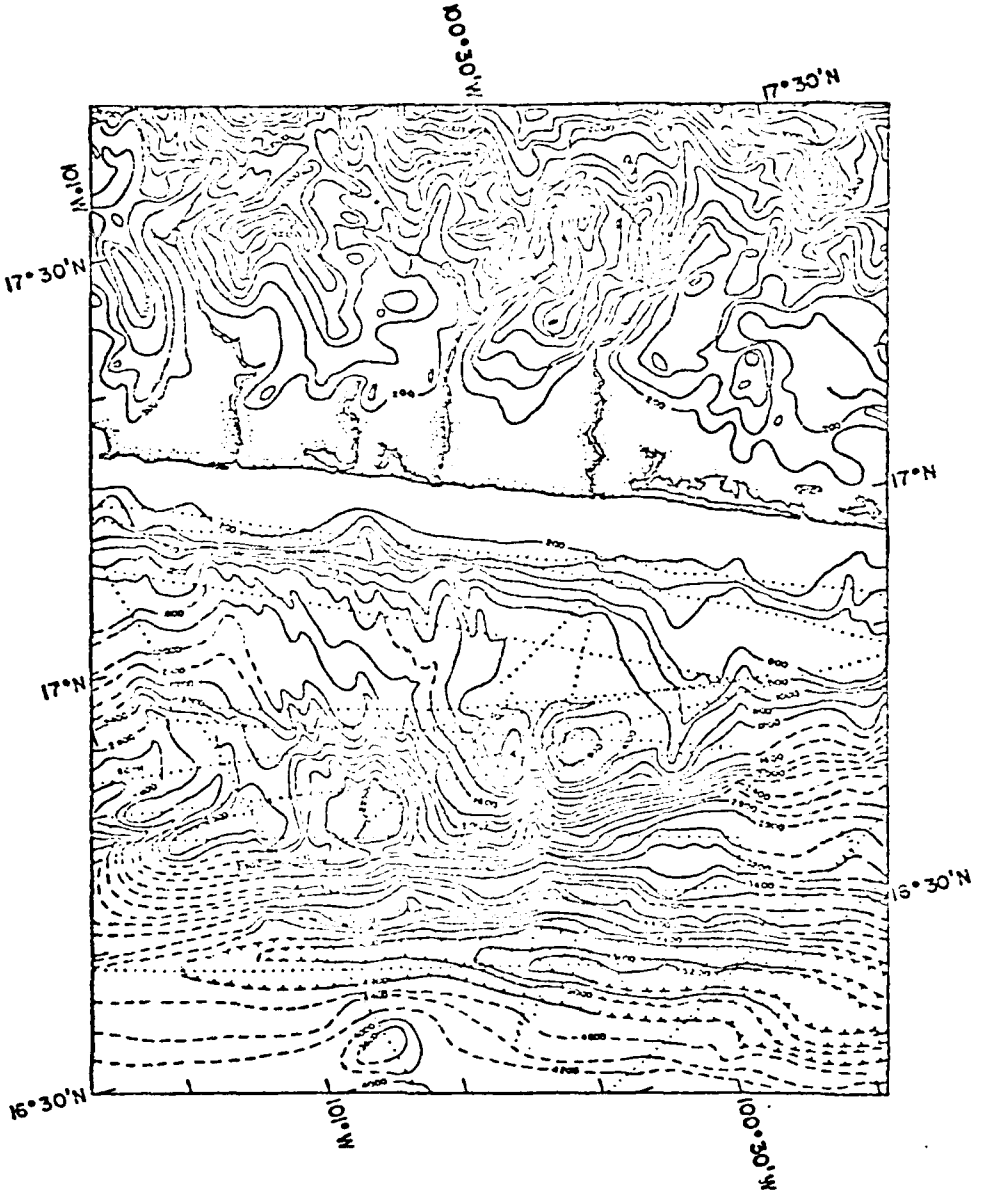

Figure 6. Bathymetric map of survey area (Karig et al., 1978); depths in meters, corrected with Matthew's tables. Topography, in meters, is simplified from 1:500,000 sheet.

parallel to the trench. The non-magnetic material comprising acoustic basement seaward of the edge of the continental crust was interpreted by Karig et al. (1978) to be deformed and uplifted trench-floor turbidites.

Detailed multi-channel seismic reflection data just south of Acapulco reveal structures on the lower slope and within the trench axis turbidite fill that Shipley et al. (1980) interpret as folds and thrust faults. Landward dipping reflections and structures provide further evidence of uplift and emplacement of trench turbidite fill along the continental margin of Mexico contributing to the formation of an accretionary prism (Seeley et al., 1974).

A large offset in the bathymetry at the survey area is evident in the 1000 m contour in Figure 6. This offset follows the seaward extension of a major fault mapped on land that trends roughly perpendicular to the coast and may be related to the segmentation of the oceanic plate (Figure 7).

LOCATION OF EVENTS RECORDED BY THE LAND ARRAY

The positions of the instruments in the land array are given in Table 1. The array remained in operation from June 5 to June 29, 1977 during which time a total of 163 events were recorded and located.

Due to the lack of information concerning the velocity structure of the continental crust in this area a half-space velocity model having a compressional wave velocity, V_p, of 6.3 km/s and a shear wave velocity, V_s, of 3.64 km/s was used in computing earthquake locations as suggested by Dr. Mori. The use of this model causes a bias towards

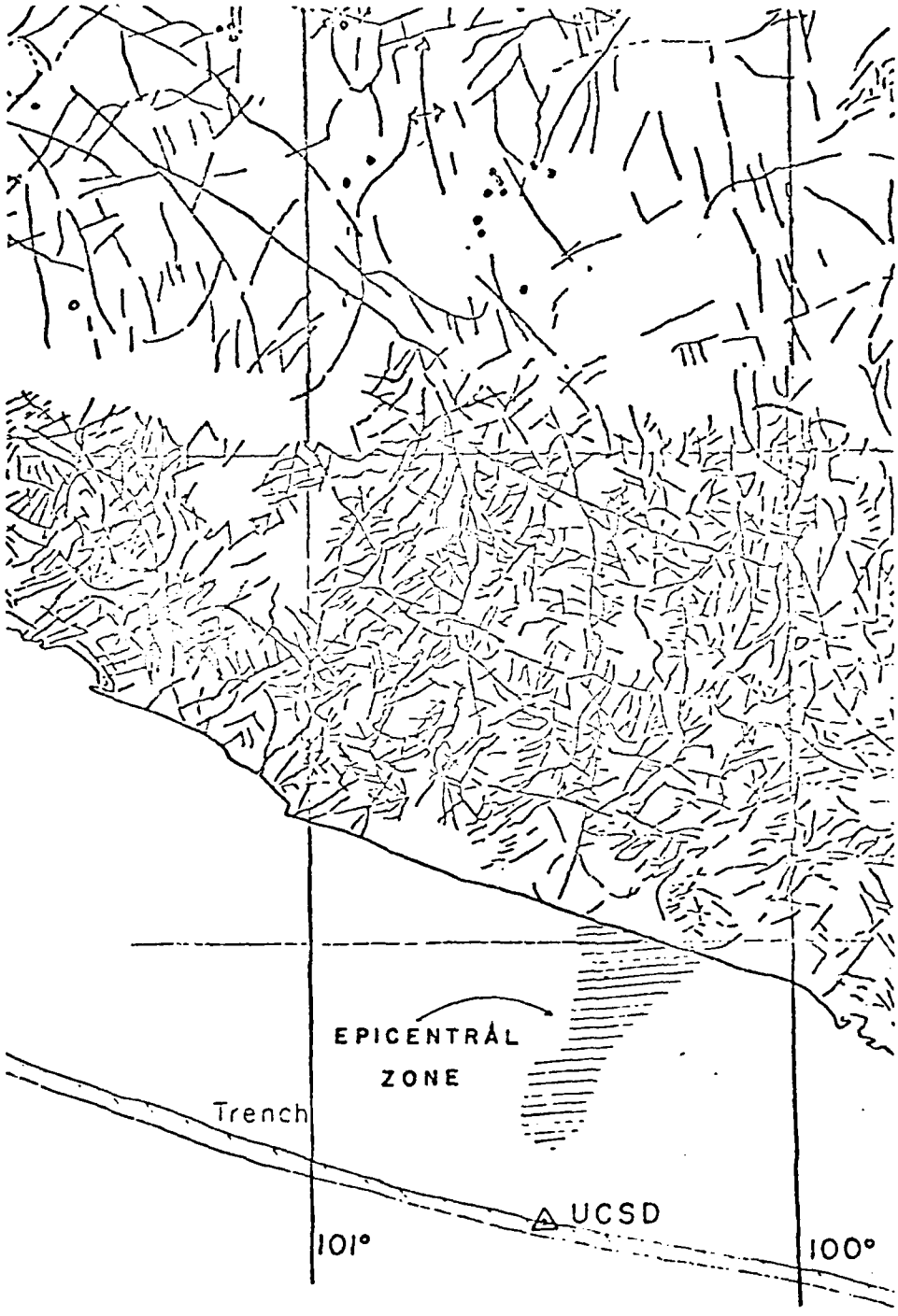

Figure 7. Location of mapped faults on land provided by Dr. Lautaro Ponce Mori. Seismically active zone offshore is indicated as well as approximate location of OBS array.

Table 1

Seismometer Locations on Land

Station	LAT (°N)	LON (°W)	Elev (m)
ABG	17.05	100.07	492
CUI	17.24	100.45	305
CUC	17.22	100.29	1148
ORI	17.20	100.14	492
RAL	17.07	100.25	525
VAI	17.15	100.39	164
YET	17.01	100.02	164

shallower hypocentral depths for events occurring below the region of the crust where these velocities are good approximations.

The calculated hypocenters and origin times of the earthquakes are given in Table 2; epicenters are plotted in Figure 8. The estimated errors in computed latitude, longitude, and depth are generally less than five kilometers for events in the vicinity of the array. The accuracy of the locations decreases with increasing distance from the stations.

There are two patterns in the spatial distribution of the epicenters. The majority of the events occur randomly on land and up to about 20 km offshore, roughly the distance at which Karig et al. (1978) suggest the continental plate terminates. Further offshore the activity is restricted to a salient approximately perpendicular to the trench in line with the offset in the bathymetry (Figure 8).

The temporal distribution of the events is shown in Figure 9. There are two periods of time during which there were apparently no events detected. The first one lasted about three days from June 14 to June 16 and the second lasted four days from June 20 to June 23. We do not know whether these actually were quiescent periods during the experiment or if they simply appear to be because of difficulties encountered in maintaining the array due to the isolation of the instruments in mountainous terrain. With the exception of these seven days the level of activity remained fairly constant with an average of 10 events per day.

Table 2. Location of earthquakes from land-based stations.

#	LAT	ERR	LON	ERR	DEPTH	ERR	M	D	HR	MN	SEC	ERR
1	16.89	0.65	100.21	1.50	20.4	1.6	6	5	2	3	15.37	0.22
2	16.99	0.83	100.38	1.00	16.7	1.4	6	5	4	20	24.26	0.19
3	16.56	1.50	100.47	2.50	34.2	4.6	6	5	7	26	17.58	0.22
4	16.98	2.00	99.60	1.90	4.2	18.0	6	5	8	12	42.30	0.25
5	16.88	0.84	100.04	1.30	23.8	1.4	6	5	8	35	59.79	0.19
6	17.14	0.73	100.15	1.10	39.0	1.3	6	5	8	39	41.92	0.21
7	17.15	0.78	100.17	1.20	43.6	1.2	6	5	9	51	51.10	0.19
8	16.87	0.68	100.18	1.30	25.1	1.0	6	5	12	42	52.64	0.19
9	16.87	0.65	100.22	1.20	21.9	1.7	6	5	13	2	2.01	0.18
10	16.97	0.74	100.33	1.10	26.3	1.3	6	5	14	4	39.50	0.18
11	17.03	1.50	99.67	1.70	31.7	1.8	6	5	14	34	52.70	0.20
12	17.08	0.90	100.17	1.20	31.1	1.4	6	6	1	26	50.86	0.22
13	17.72	2.50	99.76	6.50	13.4	35.0	6	6	1	56	19.59	0.31
14	17.09	0.68	100.18	0.82	12.4	1.4	6	6	5	36	15.73	0.21
15	18.15	3.40	100.96	5.10	57.2	11.0	6	6	8	3	2.21	0.22
16	16.67	2.90	99.61	4.20	85.0	3.9	6	6	8	26	10.25	0.22
17	17.00	2.70	99.66	3.00	51.1	3.7	6	6	9	10	48.34	0.43
18	16.97	0.83	100.32	1.40	24.3	1.4	6	6	10	17	50.55	0.22
19	17.68	2.60	100.70	3.50	59.8	4.9	6	6	10	22	39.92	0.43
20	16.98	1.10	100.08	1.30	18.2	1.7	6	6	10	26	32.27	0.22
21	17.01	3.30	101.27	4.10	48.4	6.4	6	6	10	51	30.55	0.30
22	16.95	1.10	100.16	1.60	36.4	1.5	6	6	11	13	49.22	0.22
23	17.17	1.00	100.15	1.40	38.1	1.3	6	6	11	38	46.84	0.22
24	16.91	1.20	100.46	1.70	29.1	1.7	6	6	12	5	21.88	0.22
25	17.29	2.60	101.09	3.50	48.4	4.4	6	6	15	34	21.25	0.22
26	17.06	2.00	100.83	2.50	39.1	2.6	6	6	18	41	45.06	0.22
27	17.19	0.67	100.30	0.89	12.1	2.8	6	6	20	55	3.28	0.35
28	16.93	1.60	100.35	1.60	23.0	1.7	6	6	20	58	27.38	0.26
29	16.80	1.10	100.19	1.80	11.5	4.5	6	7	0	32	18.49	0.22
30	17.05	1.90	99.72	2.00	12.2	7.2	6	7	0	37	0.33	0.22
31	17.04	0.92	100.30	1.30	34.7	1.4	6	7	0	52	33.76	0.22
32	17.06	1.20	100.02	1.10	15.0	1.8	6	7	3	49	8.72	0.22
33	16.80	1.90	99.76	2.50	25.7	5.5	6	7	4	27	2.21	0.22
34	16.84	2.80	99.47	4.00	65.0	4.6	6	7	4	41	21.83	0.25
35	17.28	2.90	99.82	2.70	61.9	2.3	6	7	4	57	13.34	0.26
36	17.14	1.90	100.07	1.80	46.2	1.6	6	7	5	26	42.35	0.26
37	16.96	0.86	100.33	1.40	24.3	1.4	6	7	5	34	22.35	0.22
38	17.10	1.10	100.11	1.40	35.4	1.4	6	7	5	52	25.56	0.22
39	17.00	0.86	100.31	1.30	28.8	1.4	6	7	7	41	38.72	0.22
40	17.01	0.83	100.39	1.20	14.2	1.5	6	7	8	21	36.33	0.22
41	17.05	0.85	100.39	1.10	20.1	1.3	6	7	8	23	1.50	0.22

Table 2 (cont.)

#	LAT	ERR	LON	ERR	DEPTH	ERR	M	D	HR	MN	SEC	ERR
42	17.55	3.70	100.70	3.40	71.6	3.5	6	7	9	6	35.21	0.26
43	17.06	1.30	100.18	1.20	28.6	1.6	6	7	9	55	13.20	0.26
44	17.36	4.50	98.99	6.30	97.3	5.5	6	7	13	41	22.44	0.31
45	17.17	0.91	100.20	1.30	36.1	1.4	6	7	14	32	2.71	0.22
46	17.14	1.10	100.14	1.40	38.6	1.4	6	7	14	35	24.22	0.22
47	17.20	2.90	100.38	1.80	8.8	4.4	6	7	15	36	41.99	0.71
48	17.10	1.30	100.01	1.50	35.0	1.4	6	7	17	38	21.47	0.22
49	17.16	1.50	100.51	2.60	47.7	1.6	6	8	3	53	21.26	0.26
50	17.16	1.00	100.41	1.40	21.0	1.5	6	8	4	35	53.31	0.26
51	17.03	1.90	99.87	2.60	38.5	2.3	6	8	5	20	32.88	2.60
52	17.17	1.00	100.30	1.90	39.8	1.6	6	8	7	27	40.71	0.26
53	17.06	1.70	99.94	1.70	9.5	4.6	6	8	7	50	10.96	0.26
54	17.09	1.50	100.02	1.60	22.2	1.7	6	8	9	56	7.96	0.26
55	16.90	2.40	99.66	3.50	32.0	5.8	6	8	10	15	4.14	0.26
56	16.90	0.94	100.29	2.10	23.9	1.9	6	8	10	29	55.30	0.26
57	17.10	2.10	99.78	3.00	41.7	2.4	6	8	12	3	11.52	0.26
58	16.75	1.30	100.51	2.30	13.1	7.4	6	9	2	55	2.54	0.26
59	17.10	1.80	99.77	2.10	33.6	2.1	6	9	5	49	30.09	0.26
60	18.07	4.80	98.63	8.20	131.6	10.0	6	9	19	10	12.12	0.26
61	17.09	2.40	99.62	7.30	38.6	5.0	6	9	21	49	40.91	0.26
62	18.02	2.40	100.71	6.00	13.7	38.0	6	10	1	37	40.31	0.31
63	17.06	0.35	100.41	2.10	24.4	1.5	6	10	4	42	23.17	0.26
64	17.36	1.30	100.59	3.00	41.8	1.8	6	10	6	29	45.00	0.26
65	17.22	1.60	100.71	3.10	39.5	1.5	6	10	11	26	35.16	0.26
66	17.28	0.72	100.32	2.30	35.4	1.8	6	10	16	4	20.31	0.26
67	17.34	6.10	100.86	6.40	7.5	25.0	6	10	16	56	8.97	0.26
68	17.40	1.10	100.49	2.90	39.6	2.1	6	10	17	35	7.51	0.26
69	17.49	1.10	100.22	2.40	15.6	5.2	6	10	21	36	46.00	0.26
70	17.17	0.75	100.22	1.20	23.3	1.7	6	10	21	49	56.34	0.26
71	17.44	2.10	100.98	4.60	37.2	3.9	6	11	17	31	17.59	0.26
72	16.98	1.40	100.59	2.80	32.8	2.3	6	11	17	42	24.57	0.26
73	17.05	0.77	100.38	2.20	26.3	1.6	6	11	23	39	19.21	0.26
74	17.02	0.84	100.40	2.20	20.1	1.7	6	12	3	7	23.04	0.26
75	17.29	1.30	100.55	2.40	34.4	1.5	6	12	4	49	24.18	0.26
76	16.97	1.50	99.88	4.70	48.7	2.8	6	12	5	12	17.33	0.26
77	17.26	1.20	100.44	0.92	7.6	1.8	6	12	7	36	32.32	0.26
78	16.91	0.80	100.38	2.70	12.5	5.0	6	12	8	20	56.55	0.26
79	16.97	1.50	100.67	3.10	33.9	2.8	6	12	9	37	9.50	0.26
80	17.21	1.10	100.07	2.90	32.1	1.5	6	12	9	56	46.08	0.26
81	17.21	2.00	99.52	5.70	11.9	9.6	6	12	12	40	17.62	0.26
82	16.83	1.50	99.95	4.90	50.1	4.0	6	12	13	11	42.04	0.26

Table 2 (cont.)

#	LAT	ERR	LON	ERR	DEPTH	ERR	M	D	HR	MN	SEC	ERR
83	17.03	0.72	100.33	2.40	30.0	1.8	6	12	13	36	48.21	0.26
84	17.11	0.98	100.11	2.80	33.3	1.6	6	13	5	31	29.73	0.26
85	17.27	2.10	100.99	4.50	41.2	2.7	6	13	6	46	29.38	0.26
86	17.00	1.10	100.48	2.20	18.5	2.1	6	13	9	12	43.89	0.26
87	17.23	1.10	100.48	2.60	41.4	1.5	6	13	9	14	36.80	0.26
88	17.10	0.95	100.12	2.90	35.6	1.7	6	13	9	15	15.87	0.26
89	16.82	1.60	99.84	5.00	41.9	5.1	6	13	9	20	38.39	0.26
90	17.20	0.64	100.28	2.20	33.3	1.7	6	13	10	11	41.23	0.26
91	17.46	1.30	100.57	2.80	28.5	2.9	6	13	10	43	3.74	0.26
92	17.16	0.84	100.25	2.90	44.8	1.6	6	13	14	37	26.98	0.26
93	16.88	1.90	99.69	5.80	49.4	4.4	6	13	15	13	56.30	0.26
94	17.48	6.60	100.66	7.30	42.3	2.3	6	16	21	26	25.02	0.26
95	17.20	3.50	100.08	4.20	7.7	16.0	6	17	2	57	35.39	0.26
96	17.37	5.10	100.00	6.10	15.5	22.0	6	17	5	31	6.22	0.26
97	17.36	3.70	100.20	4.30	19.3	9.0	6	17	6	41	21.36	0.26
98	17.29	4.50	100.21	5.30	36.8	4.7	6	17	7	13	18.28	0.26
99	20.05	11.00	100.55	12.00	23.8	42.0	6	17	9	11	51.92	0.26
100	17.09	7.80	99.67	9.40	11.8	43.0	6	17	9	14	58.81	0.26
101	17.44	5.40	100.46	6.00	39.3	3.9	6	17	12	37	20.62	0.26
102	16.88	5.00	100.68	5.80	14.5	22.0	6	17	13	12	35.69	0.26
103	17.67	6.20	100.39	7.00	14.2	27.0	6	17	13	45	55.85	0.26
104	17.24	3.80	100.09	4.60	20.3	8.6	6	17	14	56	1.68	0.26
105	17.25	6.60	100.65	10.00	39.4	3.0	6	17	16	2	52.89	0.31
106	17.41	6.20	99.90	7.40	17.0	30.0	6	17	16	16	56.05	0.26
107	17.06	3.80	100.32	4.70	34.0	1.7	6	17	18	10	7.26	0.26
108	17.04	3.50	100.31	4.40	30.4	1.7	6	17	19	10	7.67	0.26
109	18.35	14.00	100.60	16.00	40.3	45.0	6	17	19	24	2.40	0.26
110	17.12	4.60	99.99	5.60	15.0	11.0	6	17	22	47	58.00	0.26
111	16.97	4.40	100.16	5.60	30.2	1.5	6	17	23	37	19.85	0.25
112	16.79	4.70	100.51	5.80	10.8	27.0	6	18	0	2	20.89	0.25
113	16.82	5.20	100.47	6.30	32.7	8.5	6	18	0	7	10.50	0.25
114	16.82	5.00	100.49	6.10	29.0	9.5	6	18	0	29	16.00	0.25
115	17.08	5.40	100.79	5.30	9.2	27.0	6	18	0	40	45.61	0.26
116	16.97	3.10	100.48	3.90	7.6	12.0	6	18	1	42	50.40	0.25
117	17.50	7.50	100.73	8.40	48.3	2.2	6	18	1	47	15.72	0.26
118	16.78	4.80	100.51	5.90	14.4	21.0	6	18	2	27	24.14	0.26
119	17.22	3.30	100.45	4.10	32.5	1.5	6	18	3	10	43.02	0.25
120	16.79	4.50	100.44	5.70	14.3	17.0	6	18	4	27	34.32	0.26
121	16.88	4.40	100.41	5.60	29.9	6.0	6	18	5	54	0.88	0.25
122	16.78	4.90	100.52	6.00	14.1	22.0	6	18	6	31	1.65	0.26
123	16.87	4.10	100.47	5.10	19.6	9.7	6	18	7	17	42.63	0.25

Table 2 (cont.)

#	LAT	ERR	LON	ERR	DEPTH	ERR	M	D	HR	MN	SEC	ERR
124	16.78	5.00	100.55	6.10	14.0	24.0	6	18	9	4	36.49	0.26
125	16.70	5.50	100.51	6.90	14.5	28.0	6	18	10	6	0.06	0.26
126	17.06	4.20	100.30	5.20	38.6	1.6	6	18	11	8	49.89	0.26
127	17.44	7.10	100.77	7.80	43.0	2.3	6	18	11	40	34.35	0.26
128	17.29	9.50	100.64	3.70	20.0	0.0	6	18	13	5	25.79	0.93
129	16.79	6.50	100.15	8.00	43.3	4.3	6	18	15	47	57.90	0.26
130	17.01	3.20	100.36	4.20	25.4	2.4	6	18	15	51	35.67	0.26
131	16.75	5.30	100.55	6.50	17.0	22.0	6	18	16	0	31.47	0.26
132	17.18	4.80	100.50	5.30	42.4	1.8	6	18	16	1	44.32	0.26
133	16.72	5.50	100.55	6.70	13.8	29.0	6	18	22	36	11.20	0.26
134	17.15	2.50	100.27	3.30	20.0	2.6	6	18	22	58	13.49	0.26
135	16.71	5.50	100.53	6.80	10.3	40.0	6	18	23	0	9.97	0.26
136	16.75	5.50	100.49	6.80	27.9	13.0	6	18	23	24	21.41	0.26
137	17.22	2.30	100.20	3.00	8.1	9.1	6	18	23	32	51.27	0.26
138	16.74	5.50	100.52	6.80	23.4	16.0	6	19	0	14	55.19	0.26
139	16.74	5.40	100.53	6.60	17.0	23.0	6	19	0	15	22.53	0.26
140	16.74	5.40	100.54	6.60	17.0	23.0	6	19	0	23	49.32	0.26
141	16.69	5.30	100.53	7.10	14.8	31.0	6	19	2	10	6.78	0.26
142	16.69	5.70	100.49	7.00	17.0	25.0	6	19	3	30	50.34	0.26
143	17.11	4.70	100.24	5.70	43.6	1.8	6	19	4	4	13.92	0.26
144	17.41	5.70	100.49	6.30	44.5	2.9	6	19	6	24	18.74	0.26
145	16.98	4.00	100.45	4.90	31.4	3.9	6	19	9	37	1.31	0.26
146	17.06	2.60	100.35	3.50	20.6	1.7	6	19	13	26	53.44	0.26
147	17.19	3.40	100.36	3.90	30.6	1.9	6	19	13	27	47.55	0.26
148	17.26	4.40	100.45	4.90	39.0	1.6	6	24	3	36	45.16	0.26
149	17.06	3.70	100.21	4.70	29.1	1.6	6	24	23	42	59.29	0.26
150	17.19	0.37	100.33	0.43	34.2	0.2	6	25	0	44	4.24	0.26
151	16.59	8.20	100.08	9.50	17.7	21.0	6	25	5	13	16.17	0.31
152	17.13	4.30	100.28	5.10	39.9	1.7	6	25	9	54	50.67	0.26
153	16.89	4.90	100.31	6.20	37.5	4.0	6	25	10	50	30.68	0.26
154	16.71	6.30	100.51	7.70	35.0	13.0	6	25	12	18	50.69	0.26
155	17.25	1.40	100.29	1.60	35.9	1.6	6	26	22	53	12.65	0.26
156	17.30	1.90	100.48	1.90	32.5	2.5	6	27	9	25	20.35	0.26
157	17.06	0.67	100.13	0.75	13.5	1.9	6	27	14	13	29.26	0.26
158	17.13	1.10	100.23	1.20	32.0	1.6	6	27	14	59	28.91	0.26
159	17.14	1.50	100.38	1.30	24.2	1.6	6	27	15	48	56.74	0.26
160	18.15	3.80	100.47	6.90	16.6	43.0	6	29	0	15	43.06	0.22
161	17.17	1.60	100.43	2.10	27.1	1.3	6	29	1	0	35.25	0.22
162	17.45	1.60	100.33	2.60	23.5	4.1	6	29	15	40	35.17	0.22
163	17.48	1.90	100.44	3.10	29.5	3.4	6	29	16	23	27.41	0.22

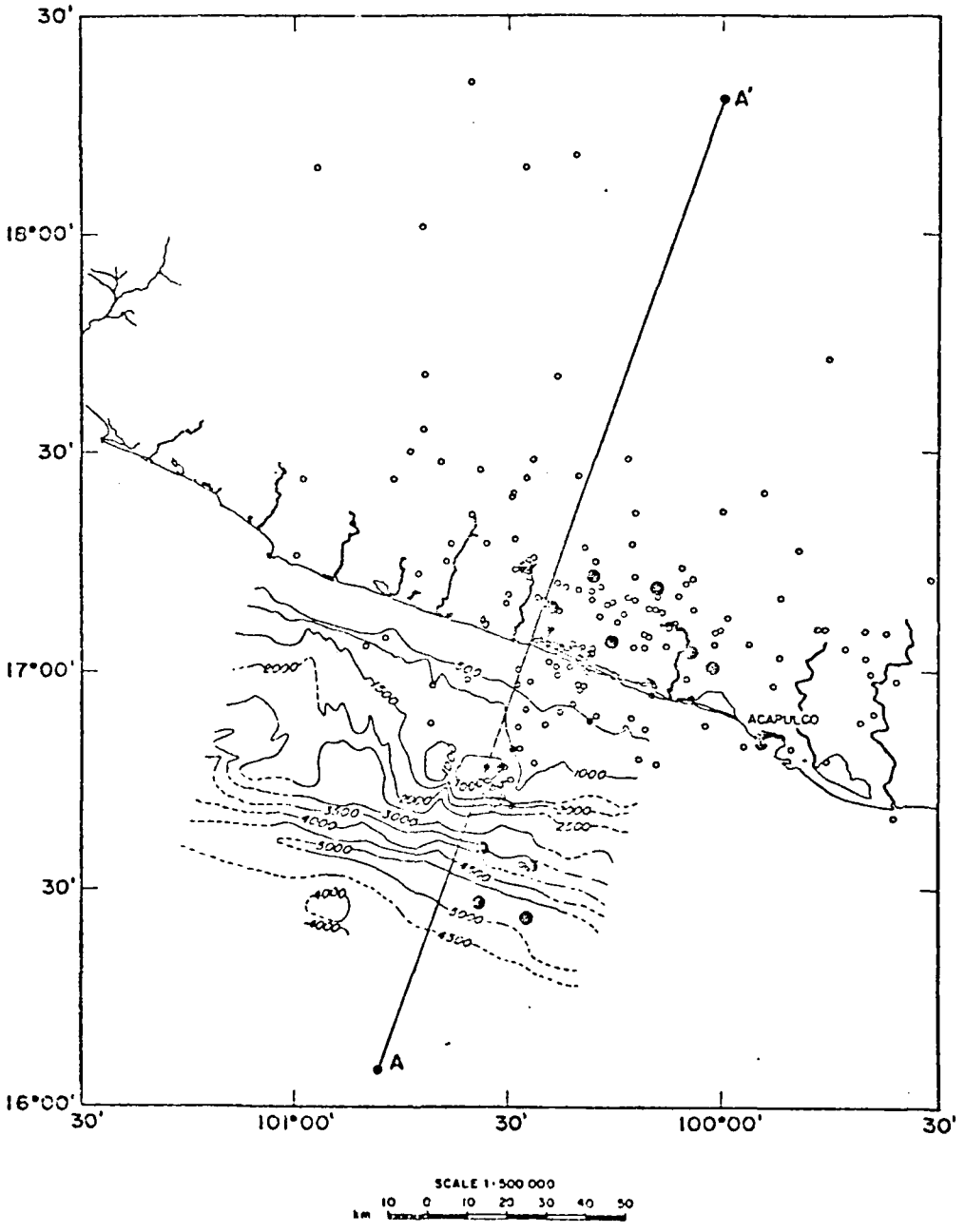

Figure 8. Epicenters (open circles) located by land-based array. Solid dots indicate locations of land-based instruments and OBS's. Bathymetry, in meters, after Karig et al. (1978).

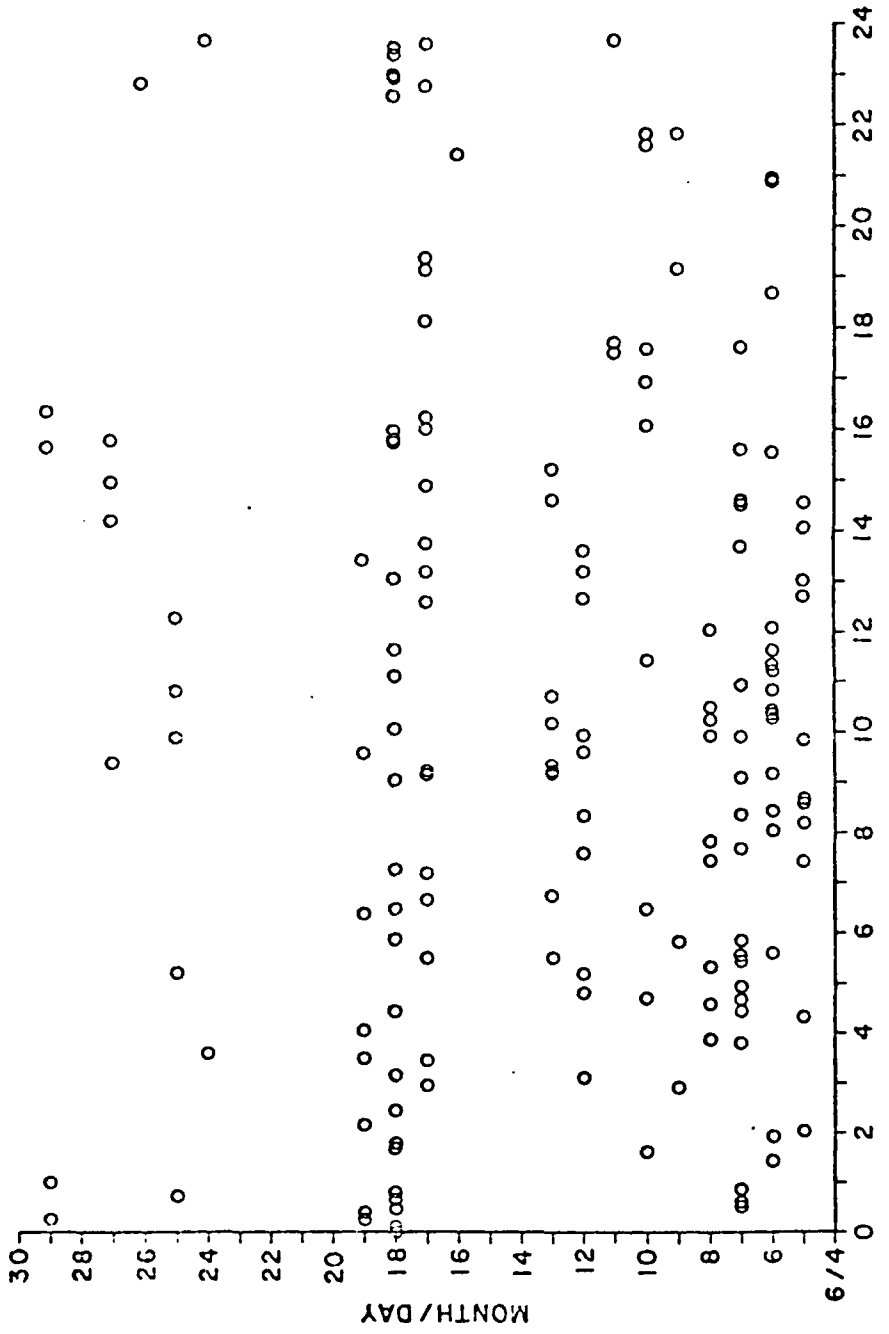

Figure 9. Origin time of events located by land-based array plotted as open circles.

THE OBS ARRAY

The OBS array operated for a little over three weeks from June 6 to July 2 (Table 3). Three of the capsules returned data for the entire period; OBS Doe returned data for only 11 days because of a trigger malfunction which exhausted her tape capacity.

The positions of the OBS's on the bottom were determined by acoustic ranging both after deployment and before recovery. The ship locations during the ranging are given in Table 4 and the corresponding two-way travel times are listed in Table 5. The computed OBS locations are in Table 6 and are plotted with respect to the ship positions in Figure 10.

The survey site was well suited for the seismicity experiment because of low noise levels. The OBS's have a variable memory buffer (4-12s) which captures a sample of the ambient bottom noise unsullied by the noise due to the tape recorder operation. During OBS experiments the recorder is periodically turned on at pre-set intervals, thus providing a number of samples of seismic noise. Amplitude spectra of ocean bottom noise samples at various past survey sites show similar characteristics. In most cases the noise level rolls off rapidly ($\sim\omega^{-4}$ - ω^{-5}) out to 2-4 Hz and much less rapidly ($\sim\omega^{-\frac{1}{2}}$) beyond about 4 Hz. Table 7 summarizes spectral amplitude measurements made by Dr. John Orcutt of Scripps of seismic noise recorded at six different OBS drop sites. The axis of the Middle America Trench is the second quietest site occupied. Noise levels on the sediment wedge are

Table 3.
Deployment and Release Times

Capsule	DEPLOYED Mon/Day	DEPLOYED Hr/Min	RELEASED Mon/Day	RELEASED Hr/Min	Days on the Bottom	Number of Records
Deni	06 09	06 26	07 02	01 43	22.8	338
Doe	06 09	00 35	07 02	07 41	23.3	654
Gwen	06 07	02 45	07 01	10 47	24.3	431
Inez	06 07	14 40	07 02	13 20	25.0	377

Table 4.
Ship Positions

Fix	Mon/Day	Hr/Min	LAT (°N) Deg / Min	LON (°W) Deg / Min
1	06 09	07 24	16 31.88	100 25.37
2	07 01	03 50	16 32.93	100 27.71
3	07 01	05 36	16 33.87	100 24.28
4	07 01	06 00	16 34.35	100 25.22
5	07 01	17 02	16 33.96	100 25.69
6	06 09	07 17	16 31.90	100 25.50
7	07 01	16 58	16 33.90	100 25.80
8	06 07	15 28	16 25.64	100 26.91
9	06 07	17 16	16 24.66	100 27.44
10	07 01	19 12	16 25.78	100 29.33
11	07 02	10 04	16 26.41	100 27.31
12	07 01	18 47	16 25.50	100 28.30
13	07 01	19 13	16 25.80	100 29.40
14	07 02	09 58	16 26.40	100 27.40
15	07 02	10 06	16 26.40	100 27.30
16	06 07	03 48	16 27.84	100 32.65
17	06 08	16 20	16 26.96	100 34.17
18	07 01	07 32	16 29.08	100 34.25
19	07 01	14 42	16 36.69	100 32.49
20	07 01	13 56	16 35.70	100 33.60
21	07 01	14 00	16 35.70	100 33.40
22	07 01	14 17	16 35.70	100 32.80

Table 5.

TWO-WAY TRAVEL TIME (s)

Fix	Deni	Doe	Gwen	Inez
1	6.310	-	-	-
2	5.905	-	-	-
3	6.920	-	-	-
4	6.455	-	-	-
5	5.583	-	-	-
6	6.181	-	-	-
7	5.490	-	-	-
8	-	-	-	7.540
9	-	-	-	7.865
10	-	-	-	9.536
11	-	-	-	7.498
12	-	-	-	8.652
13	-	-	-	9.570
14	-	-	-	7.526
15	-	-	-	7.495
16	-	-	7.777	-
17	-	-	8.129	-
18	-	-	7.827	-
19	-	5.709	-	-
20	-	5.170	-	-
21	-	5.137	-	-
22	-	5.108	-	-

Table 6.

OBS Positions

OBS	LAT (°N)	LON (°W)	Depth (m)	Semi-major† axis (km)	Semi-minor† axis (km)	Azimuth§
Deni	16.55	100.44	3830	0.4	0.2	153.00
Doe	16.60	100.55	3744	0.6	0.3	45.63
Gwen	16.47	100.56	5541	0.8	0.5	59.61
Inez	16.44	100.45	5549	0.7	0.4	165.64

† 95% confidence ellipse
§ azimuth of the semi-major axis in degrees

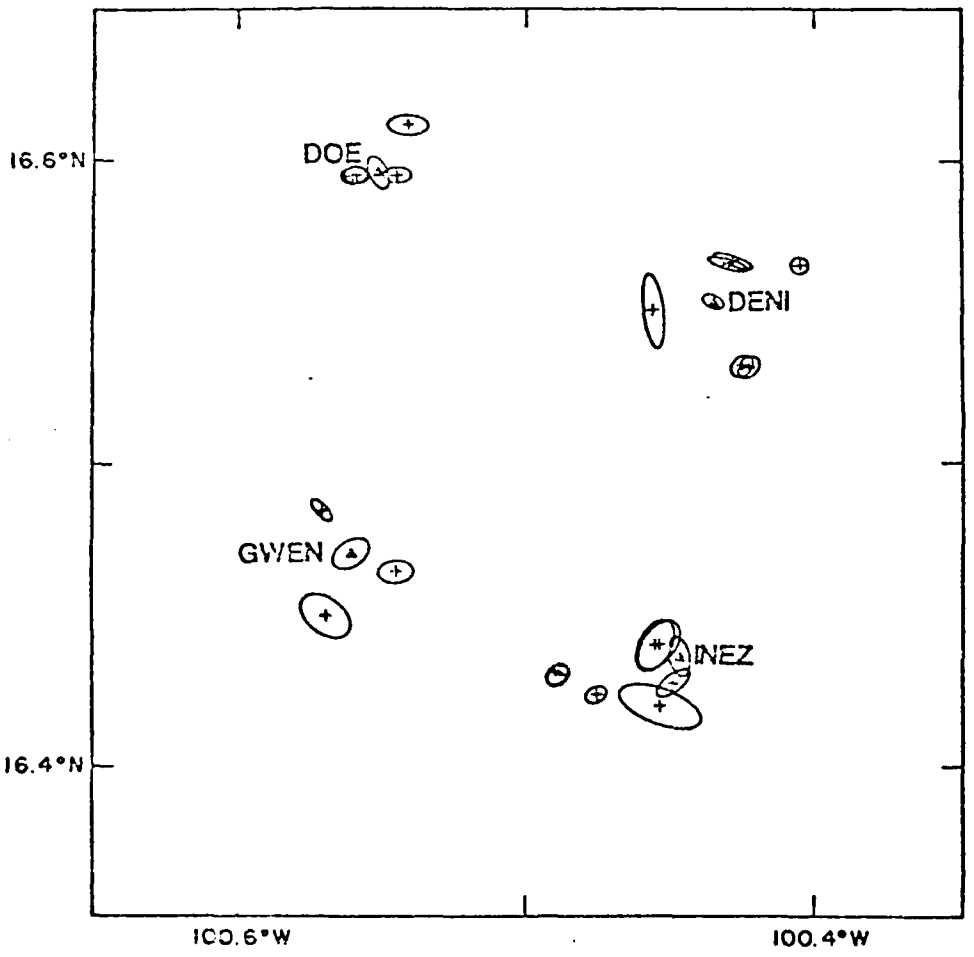

Figure 10. OBS (solid triangles) and ship (crosses) positions during ranging to OBS's along with their 95% confidence ellipses.

Table 7. Spectral amplitude measurements of seismic noise. Units are nanometers/$Hz^{\frac{1}{2}}$. The sites are arranged in order of descending noise level.

Survey Site	1 Hz	4 Hz	10 Hz
Gorda Rise	767 ± 237	3.2 ± 1.5	1.17 ± 0.6
East Pacific Long Line	270 ± 92	1.6 ± 0.4	0.4 ± 0.1
DEEPSONDE II (9°N)	132 ± 34	1.4 ± 0.2	0.16 ± 0.02
Middle America Trench: Sedimentary Wedge	110 ± 7	4.0 ± 0.1	1.1 ± 0.1
Middle America Trench: Trench Axis	60 ± 14	0.9 ± 0.5	0.4 ± 0.2
RISE (21°N)	56 ± 15	0.7 ± 0.1	0.2 ± 0.05

substantially higher however. The estimated magnitude detection threshold for events occurring within about 10 km of the array based on these noise levels is about $M_L = 0.5$.

OBS TIMING CORRECTIONS

Accurate relative timing between instruments is critical for computing earthquake locations. Late in the experiment Deni, Gwen, and Inez recorded a teleseism that occurred in the Tonga Trench at a distance of about 83°. The arrival times of the P wave from this event provided a means for assessing the relative timing errors between these three capsules. The timing of OBS Doe could not be checked because she was unable to record the teleseism having already exhausted her tape supply. The records of this event from capsules Deni, Gwen, and Inez are shown in Figure 11.

The observed arrival times of the P waves and the predicted times based on the Herrin (1968) travel time tables are compared in Table 8. The predicted times include corrections for differences in station elevation assuming a velocity of 6 km/s. Approximately 0.33s of the difference between Deni's and Gwen's residuals can be attributed to Deni's location on the accretionary prism, 1.8 km shallower than Gwen, which has an estimated average compressional wave velocity of 2.9 km/s based on sediment density versus depth (Hamilton, 1976) and velocity versus density relations (Nafe and Drake, 1963) rather than the 6 km/s used in the elevation correction. This leaves a difference in residuals of 0.76 s attributed to relative clock errors. Both Gwen and Inez were located in the trench axis at

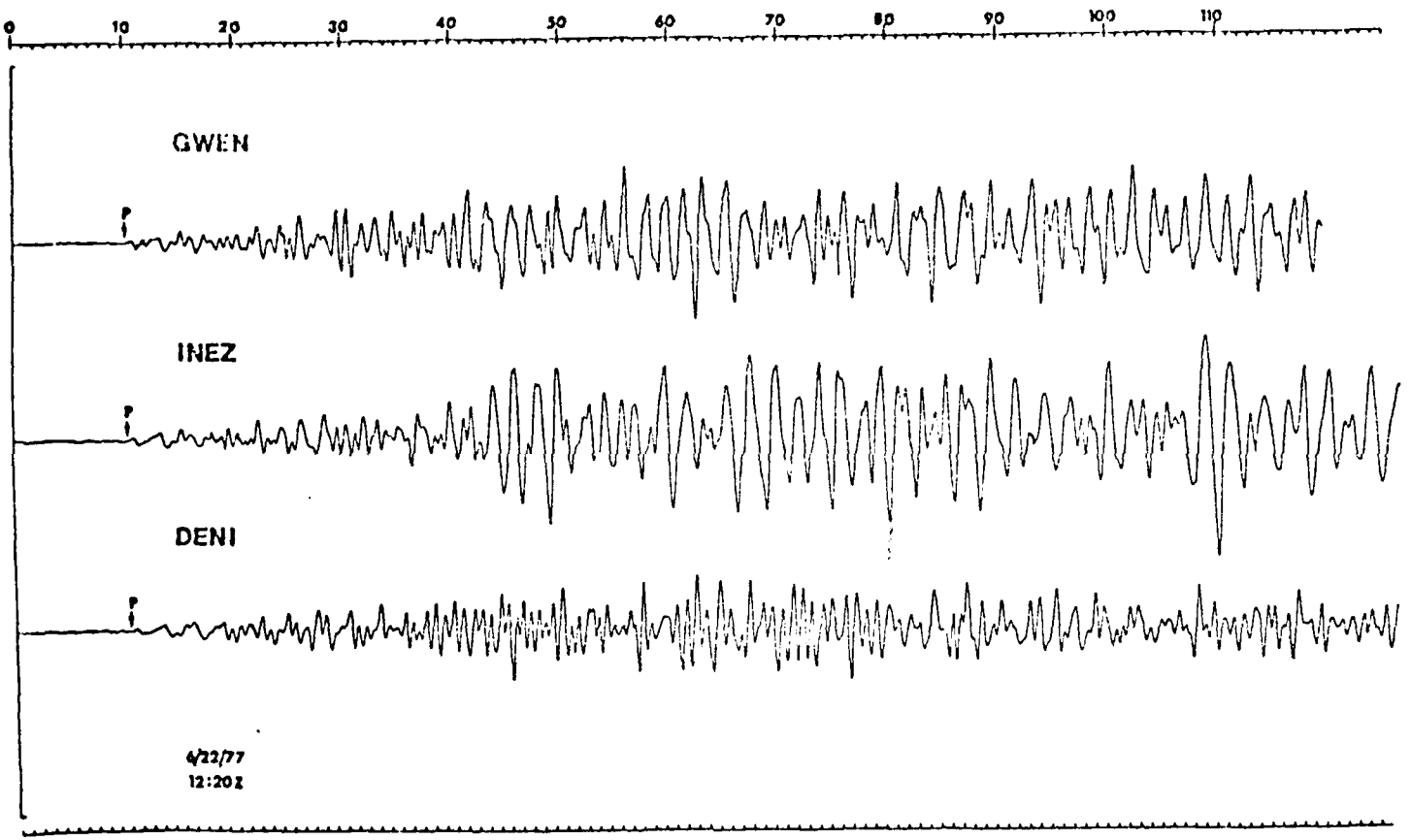

Figure 11. OBS records from event 19 on June 22, 1977, located at a distance of approximately 83° in the Tonga-Fiji area. This teleseism had a surface-wave magnitude of 7.2. Location of P wave noted; first motion is up, representing dilatation, since the polarity of the plot is reversed from true ground motion.

Table 8.

Teleseism P-wave Residuals

OBS	Observed P time (s)	Predicted* P time (s)	Residual	Relative Residual W/R to Gwen
Deni	55.43	53.79	1.64	1.09
Gwen	53.32	52.77	0.55	0.00
Inez	55.78	53.19	2.59	2.04

*Using the 1968 Herrin travel time tables

similar depths (Table 6), consequently the entire 2.04 s difference in their residuals is probably due to relative timing problems. An error of this size between Gwen and Inez is also suggested by the P and S arrival times from event 21 which occurred about 10 hours after the teleseism was recorded. While the S-P time at Inez from event 21 was only 0.28 s greater than the S-P time at Gwen, the apparent arrival time of the P wave at Inez was 2.58 s later than at Gwen suggesting a relative timing error on the order of 2 s.

Absolute errors in capsule timing of a few seconds or less can easily accumulate over lengths of time that are typical for OBS experiments. Laboratory tests have demonstrated that temperature changes similar to those induced when the capsules descend from the sea surface to the bottom can cause the OBS clock periods to decrease by as much as 1 part in 10^6. This results in an apparent increase in absolute time as measured by the OBS of 0.1 s per day.

Drift rates of the clocks in Deni and Inez relative to Gwen were computed assuming there were no timing errors when each capsule clock was reset before deployment (Table 9) and that the relative errors were 0.76 s and 2.04 s, respectively, when the teleseism was recorded. The calculated drift rates for Deni and Inez are 0.06 s/day and 0.14 s/day.

LOCATIONS AND CHARACTERTISTICS OF THE EVENTS RECORDED BY THE OBS ARRAY

The OBS array recorded a total of 24 events in addition to the teleseism, but only two of the events could

Table 9.
OBS Clock Reset Times

Capsule	Mon/Day	Lab Clock Reset Time Hr / Min	Lab Clock Drift W/R WWV (s)	Actual Reset Time Hr / Min / Sec
Deni	06 09	06 06	+0.133	06 06 0.133
Doe	06 08	23 33	+0.124	23 33 0.124
Gwen	06 07	02 18	+0.058	02 18 0.058
Inez	06 07	14 03	+0.075	14 03 0.075

be located by the OBS array. These are event numbers 2 and 21. Records of these events are shown in Figures 12 and 13. Clear P and S phases are present on all records with the exception of the seismogram from Gwen of event 2.

The seismograms show complexities not observed in land-based records of local events. One obvious complexity is the presence of compressional phases representing energy multiply reflected within the water column; these are identified by the symbol pWn in the figures. There is also a striking difference between the seismograms recorded by the OBS's in the trench axis (Gwen and Inez) and those on the accretionary prism (Deni and Doe). The record from Deni for event 21, for example, shows a complex, high-amplitude wavetrain following S not seen on either Gwen or Inez. These differences are probably due to variations in sediment thickness, which varies from a few hundred meters in the trench axis to over 1500 meters at sites on the inner trench slope (Karig et al., 1978)

Arrival times of the P and S waves of events 2 and 21 are given in Table 10 and the final locations are listed in Table 11 and plotted in Figure 14. Although both of these events were also recorded by some elements of the land array no attempt was made to incorporate arrival times at the land stations into the location process because of the extreme lateral heterogeneity between the two arrays.

The event epicenters are both located within the OBS array, event 2 in the trench axis and event 21 on the inner trench wall.

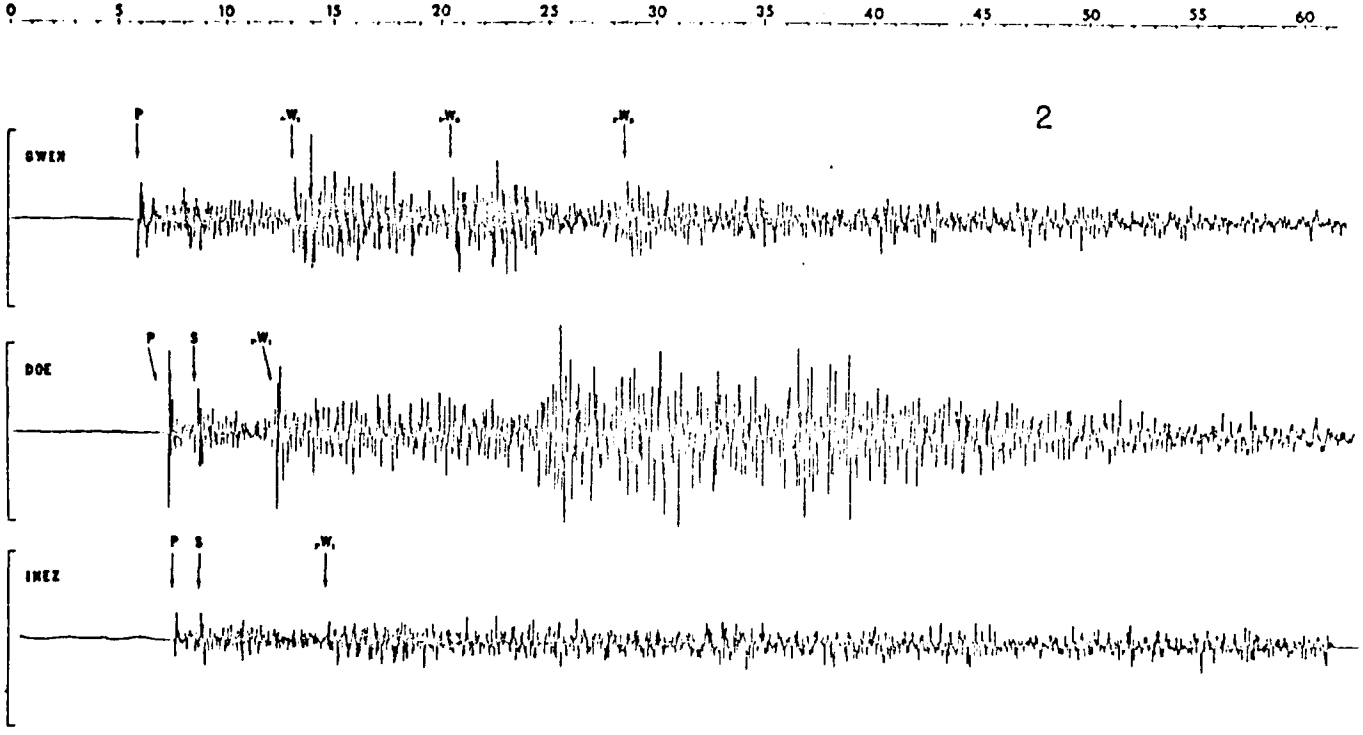

Figure 12. OBS records from event 2 on June 10, 1977 located in the trench axis at a depth of about 1 km (M_L = 2.2); location of P and S phases noted as well as water multiples ($_pW_n$).

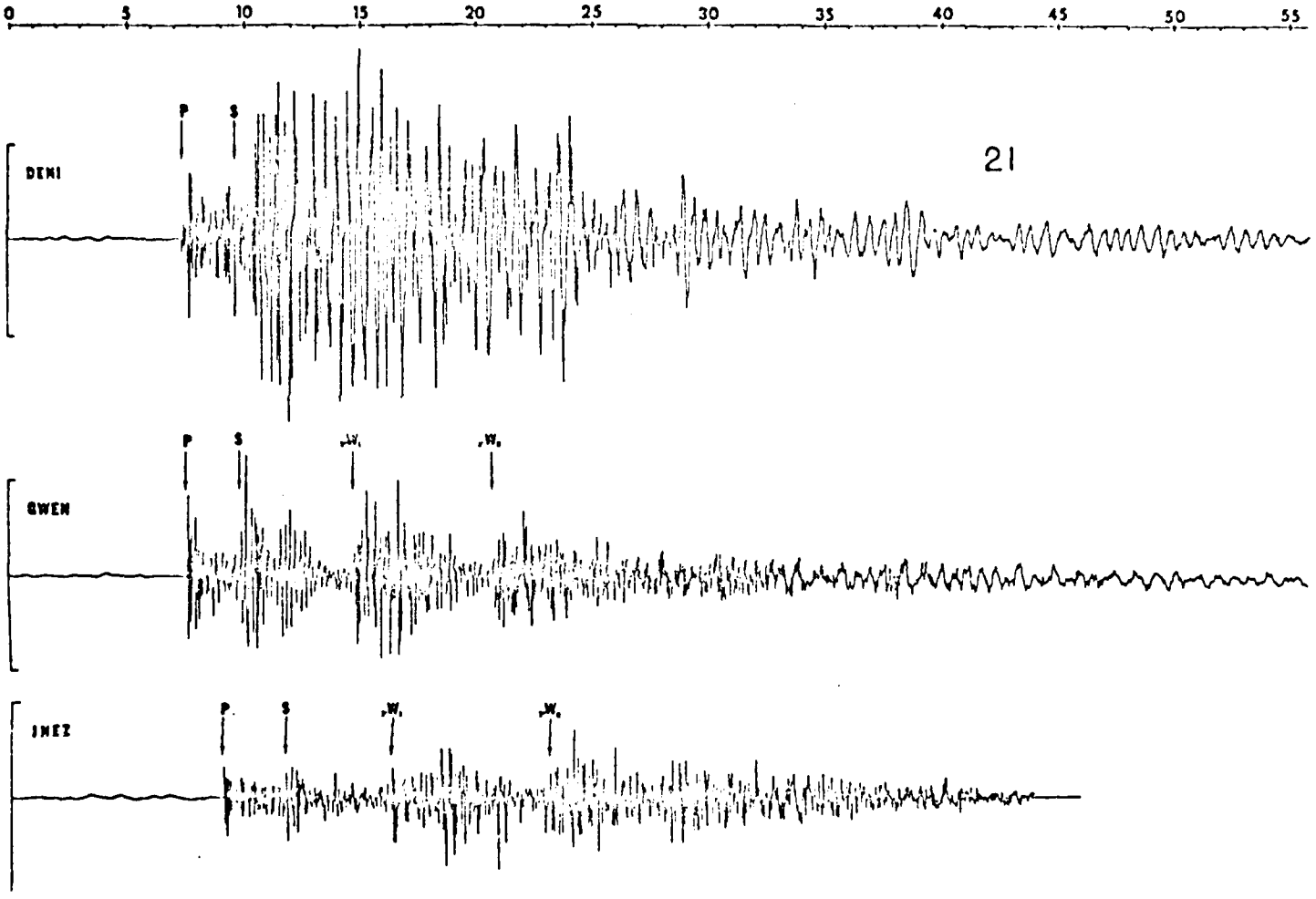

Figure 13. OBS records from event 21 on June 22, 1977 located at a depth of about 13 km beneath the accretionary prism (M_L = 2.5); location of P and S phases noted as well as water multiples ($_pW_n$).

Table 10.
P and S Arrival Times

Event	DENI				DOE				GWEN				INEZ			
	1st Mo	P	S	S-P	1st Mo	P	S	S-P	1st Mo	P	S	S-P	1st Mo	P	S	S-P
2	-	-	-	-	C	59.99	61.45	1.46	C	58.15	-	-	C	59.62	60.83	1.21
21	C	4.48	-	-	-	-	-	-	D	4.82	6.88	2.06	D	5.30	7.64	2.34

Table 11.
Event Locations From OBS Data.

Event	DATE Mon/Day	TIME Hr/Min/Sec	S.D. (s)	LAT (°N)	S.D. (km)	LON (°W)	S.D. (km)	Depth	S.D. (km)	M_L
2	06 10	21 17 57.9	0.4	16.49	2.1	100.56	1.2	0.9	22.0	2.2
21	06 22	22 45 2.1	0.4	16.56	2.7	100.51	3.1	13.0	5.7	2.5

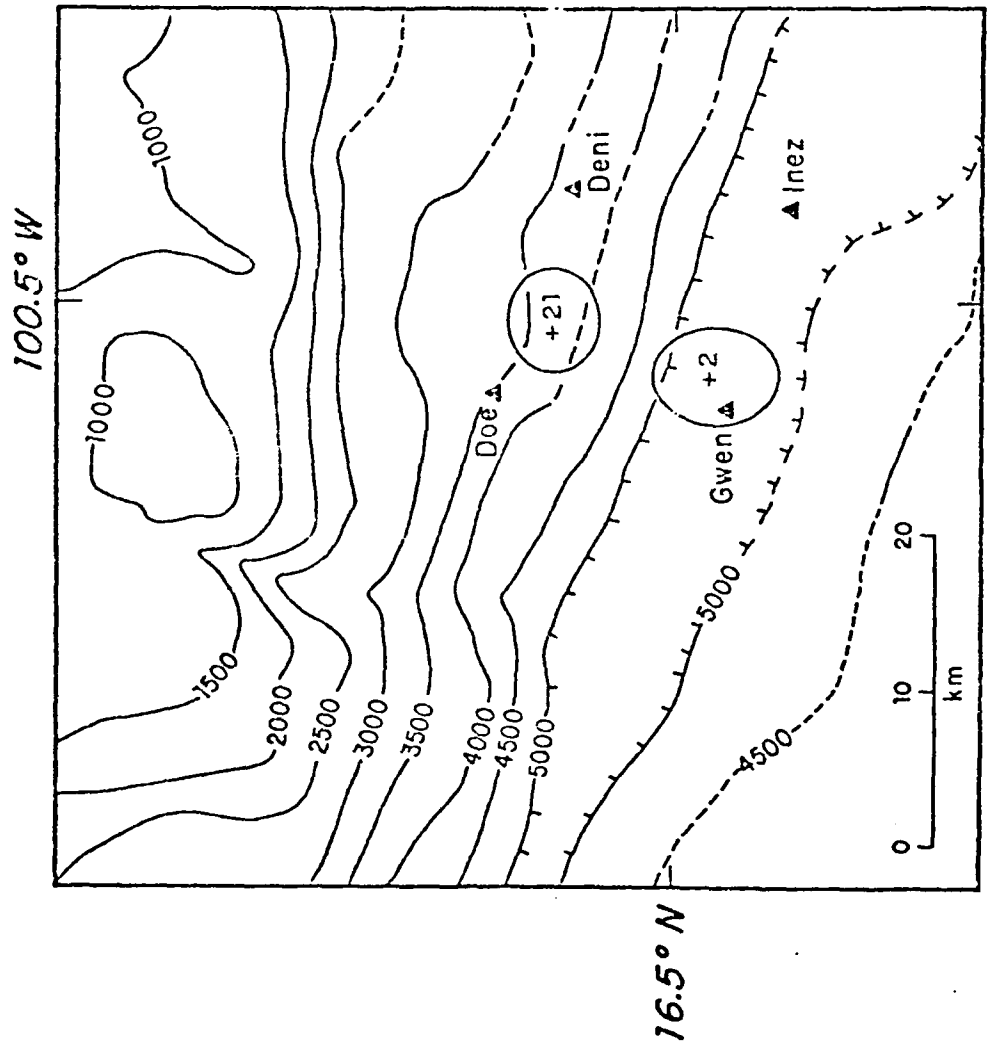

Figure 14. Epicenters of events 2 and 21 relative to the OBS array. Ellipses are 95% confidence levels; bathymetry, in meters, after Karig et al. (1978).

Event 2 appears to be very shallow but the depth is only poorly constrained (Table 11) because the arrival time of the S wave at Gwen could not be determined. The location of event 2 in the trench axis where the average sediment thickness is on the order of 500 m (Karig et al., 1978) suggests that it is located within the oceanic plate. Event 21 was located at a depth of 31 km and even within the uncertainty of the computed depth undoubtedly occurred in the subducting plate rather than the accretionary prism.

Magnitudes were calculated for both events and are given in Table 12, along with the amplitudes and frequency of the energy used in the calculation. Capsule gain settings are noted in Table 13. Final magnitudes were assigned to each event by averaging the magnitudes determined from the individual records. Both of the events were relatively small, having magnitudes of 2.2 and 2.5.

First motion data for events 2 and 21 are plotted on lower hemisphere stereographic projections in Figures 15 and 16. The direction of first motion on the OBS records is given in Table 10. Four additional first motions were obtained from elements of the land array for event 2 in the azimuth range 0° to 30° and two for event 21 in the azimuth range 0° to 15°. Because of the location of the events within the OBS array the OBS first motions were initially plotted on upper hemisphere projections assuming a constant velocity halfspace and then projected onto the lower hemisphere.

Although the available first motion data are insufficient to determine focal mechanism solutions they do provide some constraints

Table 12.

Event Magnitudes

Event	DENI				DOE				GWEN				INEZ				$\bar{M}_L$	S.D.
	A	f	Δ	M_L	A	f	Δ	M_L	A	f	Δ	M_L	A	f	Δ	M_L		
2	-	-	-	-	840	8	13.3	2.5	451	8	2.2	2.0	313	5	11.0	2.1	2.2	0.3
21	770	10	15.3	2.8	-	-	-	-	1044	4	20.4	2.9	370	15	20.4	1.9	2.5	0.6

A = maximum zero-to-peak amplitude in counts

f = signal frequency

Δ = hypocentral distance in km

M_L = local magnitude

Table 13.
OBS Gain Settings

Capsule	G' Generator constant (Volts / m/s)	A_1 Pre-amp Gain	A_o Variable Gain Setting	G Instrument Gain (counts / mm/s @ 4096 counts / 10 volts)
Deni	67.6	133.3	4	14800
Doe	81.6	275	4	36800
Gwen	59.6	400	4	39100
Inez	61.6	480	4	48400

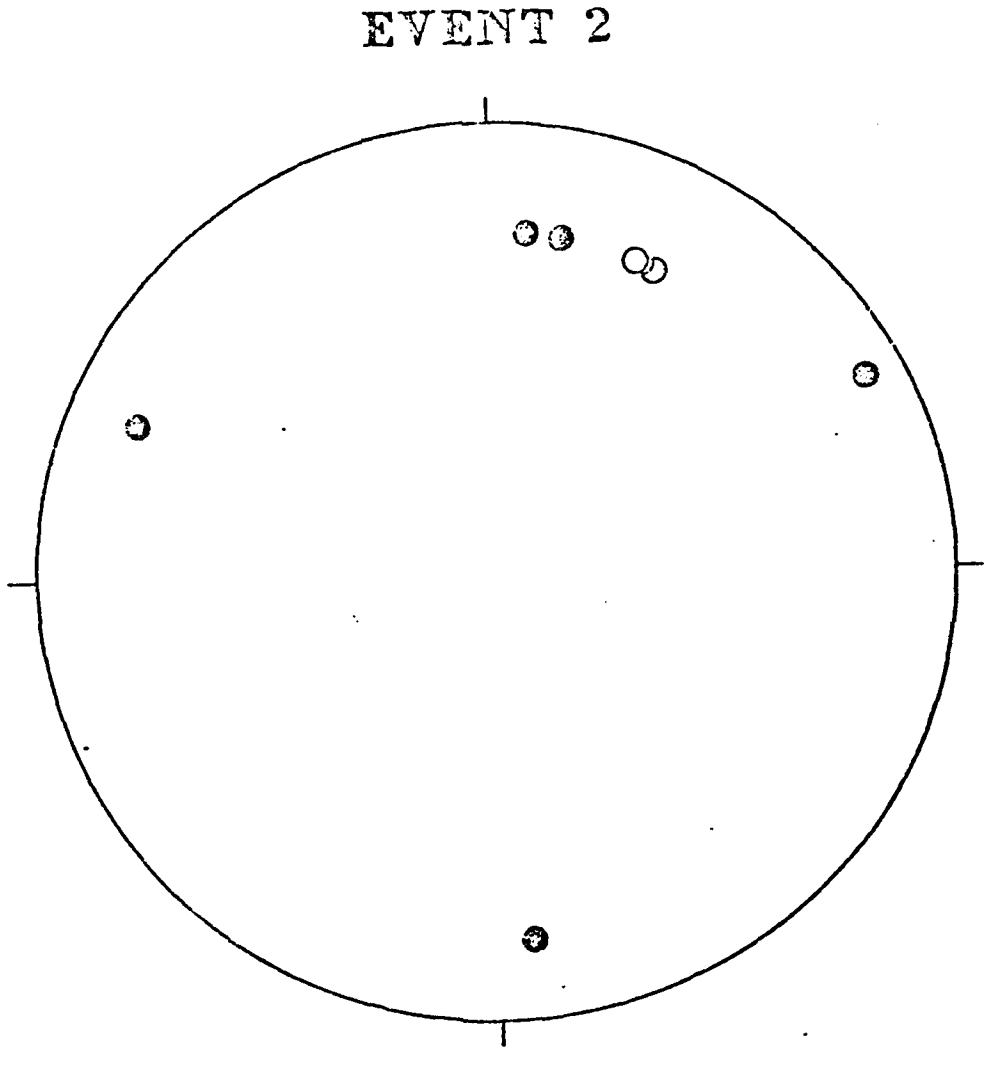

Figure 15. First motions from event 2 plotted on lower focal hemisphere; solid dots are compressions, open circles dilatations.

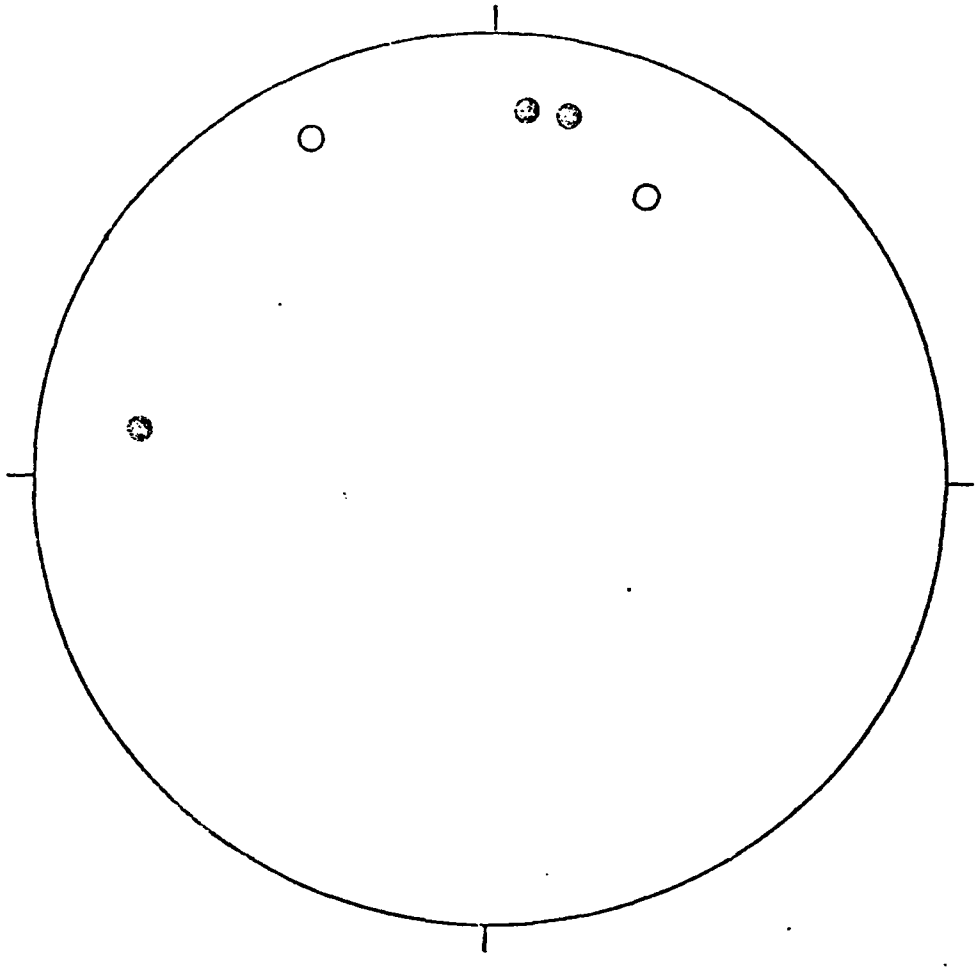

Figure 16. First motions from event 21 are plotted on lower focal hemisphere; solid dots are compressions, open circles dilatations.

on the type of faulting. The data from both events appear to be inconsistent with thrust faulting. The data from event 2 are compatible with a normal faulting mechanism having a small dip-slip component of about 20° or less oriented approximately N30°E perpendicular to the trench. The data from event 21 are compatible with normal faulting on a shallow dipping (~20°) plane roughly parallel to the trench. Although a composite focal mechanism for both events cannot be explained by a simple quadripolar pattern, the first motions from the events are not mutally inconsistent.

The data from the OBS array was insufficient to determine locations for the remaining events because too few capsules recorded them or the capsules failed to trigger on the P wave. Locations are known for four of these earthquakes, however, based on data from the land array and from a regional network of instruments across southern Mexico. Events 1, 4, and 13 were located on land using arrival time data from the land array. These earthquakes correspond to events 60, 77, and 112 in Table 2. The fourth event, number 24, was located at 16.93°N, 100.41°W at a depth of 50 km by permanent stations in southern Mexico.

Some inferences can be made concerning the locations of the remaining 18 events based on S-P times and the comparison of their waveforms with seismograms of events whose locations are known. Events 6, 8, and 16 appear as if they may have occurred close to the OBS array on the basis of S-P times of about 2 s. The accuracy of the S picks is questionable however and additional seismograms from

other capsules with S-P times of the same magnitude would be needed to assure that the identification of the S wave is correct. Events 6 and 8 occurred during the time that no events were reported from the land array, consequently there are no constraints provided by the land stations on their locations. Event 16, however, occurred during a time that events were being recorded by the land array, yet it was not detected on land. This suggests that it was located away from the land instruments, further supporting the possibility that it occurred close to the OBS array. Event 9 is known to have occurred at some distance from the OBS's on the basis of an S-P time of about 5 s recorded by capsule Doe.

The records of the remaining events are similar to those of earthquakes that were located on land such as events 1, 4, and 24. The OBS's typically triggered late on these events, probably because of relatively emergent P waves followed by energy that increased in amplitude gradually.

CONCLUSIONS

Despite the low noise level of the OBS sites (particularly in the trench axis) and resultant magnitude detection threshold of about $M_L = 0.5$, there were no events detected during the survey that definitely originated from the accretionary prism. This result is consistent with that reported by Chen et al. (1980) in an analysis of events located by OBS and land-based arrays in the New Hebrides and Central Aleutians. It appears that at our survey site the deformation of material in the accretionary prism occurs aseismically.

The level of seismic activity recorded by the OBS array was substantially lower than that recorded by the land-based instruments. The spatial distribution of the events detected during the experiment clearly indicates that the seismicity was primarily restricted to the area landward of the edge of the continental plate (Figure 8). Only a small number of events occurred further offshore in a salient extending along a line perpendicular to the trench closely following the offset in the bathymetry.

The spatial distribution of the seismicity with depth is plotted in cross section along the line A-A' on Figure 8 in Figure 17. Most of the events associated with the salient offshore have poor depth control due to their distance from the land array. The events occurring far offshore whose depths are well constrained occur within the oceanic plate.

Superimposed on Figure 17 are lines having dips of 8° extending to within about 20 km of the coast and 24° beyond that point. These lines correspond to the approximate location of the top of the oceanic plate based on the magnetic data of Karig et al. (1978) over the accretionary prism and the approximate dip of the Benioff zone based on teleseismically located events (Figure 18). Although the actual position of the top of the subducted plate may be slightly different from what is indicated in Figure 17 it is clear that the majority of the seismicity in the vicinity of the continental margin occurs in the oceanic plate with a lesser amount of activity in the overriding continental plate.

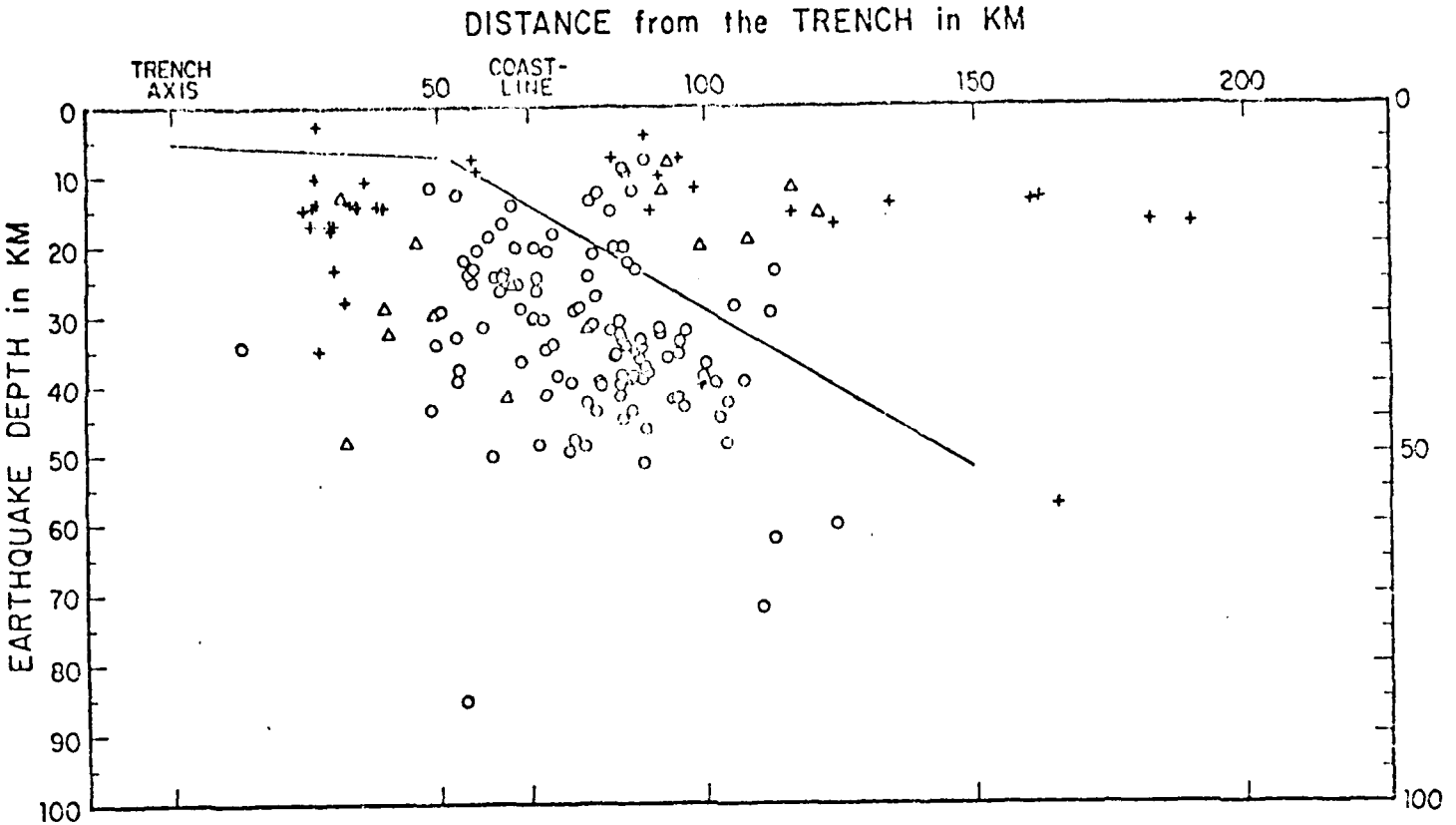

Figure 17. Event hypocenters plotted in cross section along the line A-A' in Figure 8. Standard deviations of less than 5 km (circles), 5-10 km (triangles), and more than 10 km (plusses) are indicated. Solid line corresponds to approximate location of the top the subducted oceanic plate.

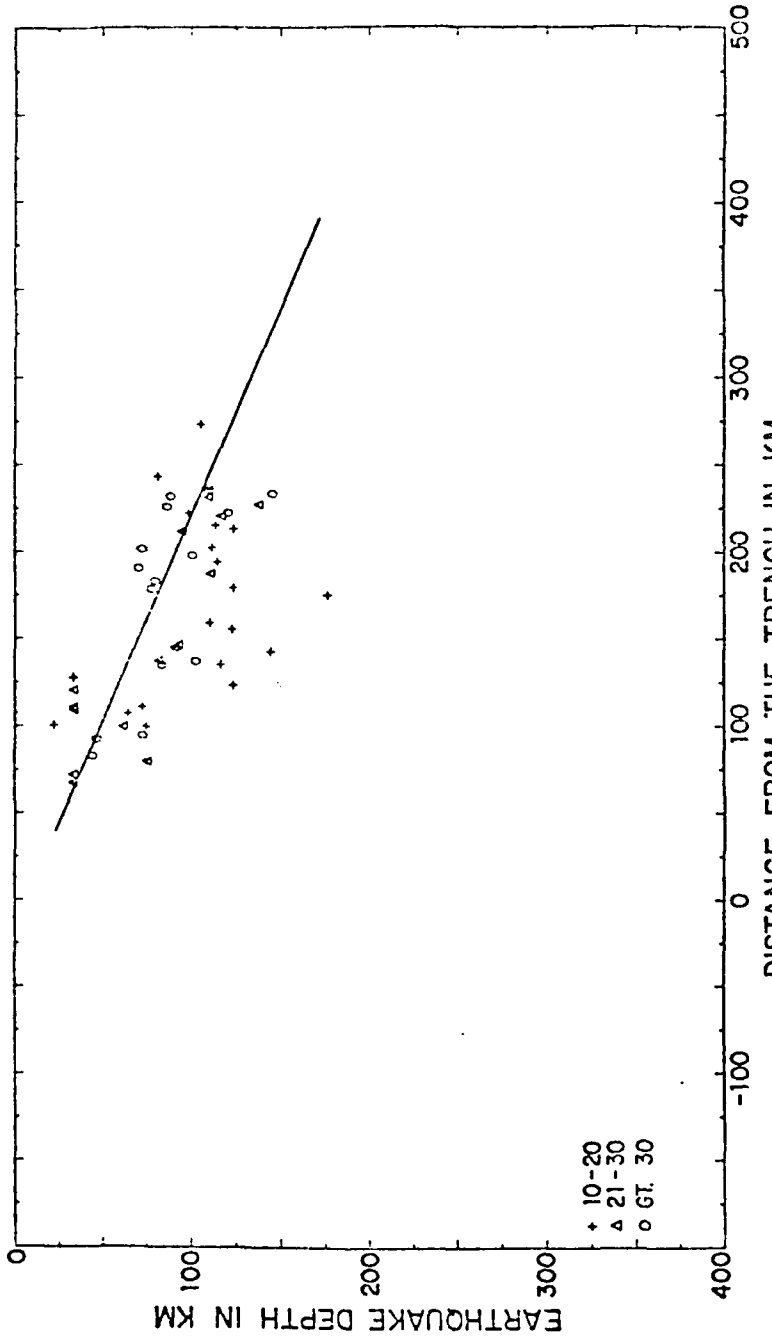

Figure 18. Hypocenters of events recorded by 10-20 (plusses), 21-30 (triangles), and more than 30 (circles) stations, in the vicinity of the study area, are projected onto a plane perpendicular to the trench. The inferred dip of the Benioff zone is approximately 24°.

The location of the salient of seismicity offshore in line with a proposed segment boundary (Figure 5) and a large fault mapped on land perpendicular to the trench (Figure 7) suggests that it may be related to tear faulting in the oceanic plate that is causing sympathetic faulting in the overriding plate. Faulting in the overriding continental plate in response to tear faults segmenting the subducted plate has been suggested by Dean and Drake (1978) in several areas along the Middle America arc. Tear faulting in the oceanic plate near the trench would be expected to result in a normal faulting mechanism oriented roughly perpendicular to the trench, consistent with the first motion data of event 2.

REFERENCES

Atwater, T.M. and J.D. Mudie (1968). Block faulting on the Gorda Rise, Science 159, 729-731.

Atwater, T. and J.D. Mudie (1973). Detailed near-bottom geophysical study of the Gorda Rise, J. Geophys. Res. 78, 8665-8686.

Bolt, B.A., C. Lomnitz and T.V. McEvilly (1968). Seismological evidence on the tectonics of central and northern California and the Mendocino escarpment, Bull. Seis. Soc. Am. 58, 1725-1767.

Buland, R. (1976). The mechanics of locating earthquakes, Bull. Seism. Soc. Am. 66, 173-187.

Carr, M.J., R.E. Stoiber and C.L. Drake (1973). Discontinuities in the deep seismic zones under the Japanese arcs, Geol. Soc. America Bull. 84, 2917-2930.

Carr, M.J., R.E. Stoiber and C.L. Drake (1974). The segmented nature of some continental margins, in Burk, C.A. and C.L. Drake, eds, The Geology of Continental Margins, Springer-Verlag, New York, 105-114.

Carr, M.J. and R.E. Stoiber (1977). Geologic setting of some destructive earthquakes in Central America, Geol. Soc. America Bull. 88, 151-156.

Chen, A.T., C. Frohlick, G.V. Latham, R.K. Cardwell and S. Billington (1980). Is there seismic activity within the accretionary prism? (abstract), Eos, Trans. Am. Geophys. Union 61, 1044.

Cox, A., R.R. Doell and G.B. Dalrymple (1963). Geomagnetic polarity epochs: Sierra Nevada II, Science 142, 382-385.

Creager, K.C. and L.M. Dorman (1980). Accurate location of ocean bottom seismograph arrays using acoustic ranging when ship position errors are covariant (abstract), Eos, Trans. Am. Geophys. Union 61, 1048.

de Cserna, Z. (1961). Tectonic map of Mexico, scale 1:2,500,000, Geol. Soc. Am., New York.

Dean, B.W. and C.L. Drake (1978). Focal mechanism solutions and tectonics of the Middle America arc, J. Geology 86, 111-128.

Dehlinger, P., R.W. Couch and M. Gemperle (1967). Gravity and structure of the eastern part of the Mendocino escarpment, J. Geophys. Res. 72, 1233-1247.

Dewey, J.W. (1972). Seismicity and tectonics of western Venezuela, Bull. Seism. Soc. Am. 62, 1711-1751.

Douglas, A. (1967). Joint epicentre determination, Nature 215, 47-48.

Fisher, R.L. (1961). Middle America Trench: Topography and structure, Geol. Soc. America Bull. 72, 703-720.

Fitch, T.J. (1970). Earthquake mechanisms and island arc tectonics in the Indonesian-Philippine region, Bull. Seis. Soc. Am. 60, 565-591.

Fowler, G.A. and L.D. Kulm (1970). Foraminiferal and sedimentological evidence for uplift of the deep-sea floor, Gorda Rise, Northeastern Pacific, J. Mar. Res. 28, 321-329.

Hamilton, E.L. (1976). Variations of density and porosity with depth in deep-sea sediments, J. Sed. Petrology 46, 280-300.

Heinrichs, D.F. (1970). More bathymetric evidence for block faulting on the Gorda rise, J. Marine Res. 28, 330-335.

Herrin, E., Chairman (1968). Seismological tables for P phases, Bull. Seis. Soc. Am. 58, 1193-1241.

Johnson, S.H. and P.R. Jones (1978). Microearthquakes located on the Blanco fracture zone with sonobuoy arrays, J. Geophys. Res. 83, 255-261.

Jones, P.R. and S.H. Johnson (1978). Sonobuoy array measurements of active faulting on the Gorda ridge, J. Geophys. Res. 3435-3440.

Karig, D.E., R.K. Cardwell, G.R. Moore and D.G. Moore (1978). Late Cenozoic subduction and continental margin truncation along the northern Middle America Trench, Geol. Soc. America Bull. 89, 265-276.

Mason, R.G. and A.D. Raff (1961). Magnetic survey off the west coast of North America, 32°N latitude to 42°N latitude, Geol. Soc. America Bull. 72, 1259-1266.

McEvilly, T.V. (1968). Seafloor mechanics of Cape Mendocino, California, Nature 220, 901-903.

McManus, D.A. (1967). Physiography of Cobb and Gorda rises, northeast Pacific Ocean, Geol. Soc. America Bull. 78, 527-546.

Menard, H.W. (1960). The East Pacific Rise, Science 132, 1737-1746.

Mooser, F. (1973). The Mexican volcanic belt: Structure and tectonics, Geofisica Internac. 13, 55-70.

Mooser, F., H. Meyer-Abich and A.R. McBirney (1958). Catalogue of active volcanoes of the world: Part VI, Central America, Internat. Assoc. Volcanology, Naples, 146 pp.

Nafe, J.E. and C.L. Drake (1963). Physical properties of marine sediments, in Hill, M.N., editor, The Sea, Vol. 3, Wiley-Interscience, New York, 794-815.

Northrop, J. (1970). Accuracy of earthquake epicenters on the Gorda ridge, Bull. Seism. Soc. Am. 60, 265-267.

Northrop, J., H.W. Menard and F.K. Duennebier (1968). Seismic and bathymetric evidence of a fracture zone on Gorda ridge, Science 161, 688-690.

Raff, A.D. and R.G. Mason (1961). Magnetic survey off the west coast of North America, 40°N latitude to 52°N latitude, Geol. Soc. America Bull. 72, 1267-1270.

Richter, C.F. (1935). An instrumental earthquake magnitude scale, Bull. Seis. Soc. Amer. 25, 1-31.

Richter, C.F. (1958). Elementary Seismology, W.H. Freeman and Company, San Francisco, 768 pp.

Riddihough, R.P. (1981). Gorda plate motions from magnetic anomaly analysis, Earth Planet Sci. Letters, in press.

Ross, D.A. and G.G. Shor, Jr. (1965). Reflection profiles across the Middle America Trench, J. Geophys. Res. 70, 5551-5572.

Seeley, D.R., P.R. Vail and G.G. Walton (1974). Trench-slope model, in Burk, C.A. and C.L. Drake, eds., The Geology of Continental Margins, Springer-Verlag, New York, 249-260.

Silver, E.A. (1971). Tectonics of the Mendocino traiple junction, Geol. Soc. America Bull. 82, 2965-2978.

Shipley, T.H., K.J. McMillen, J.S. Watkins, J.C. Moore, J.H. Sandoval-Ochoa and J.L. Worzel (1980). Continental margin and lower slope structures of the Middle America Trench near Acapulco (Mexico), Mar. Geol. 35, 65-82.

Shor, G.G., Jr. (1974). Continental margin of Middle America, in Burk, C.A. and C.L. Drake, eds., The Geology of Continental Margins, Springer-Verlag, New York, 599-602.

Shor, G.G., Jr., P. Dehlinger, H.K. Kirk and W.S. French (1968). Seismic refraction studies off Oregon and northern California, J. Geophys. Res. 73, 2175-2194.

Shor, G.G., Jr. and R.L. Fisher (1961). Middle America Trench: Seismic refraction studies, Geol. Soc. America Bull. 72, 721-730.

Spiess, F.N. and R.C. Tyce (1973). Marine Physical Laboratory Deep-Tow instrument system, SIO Reference Series 73-4, Scripps Inst. Oceanography, Univ. Cal. San Diego.

Stauder, W. (1968). Mechanism of the Rat Island earthquake sequence of February 4, 1965 with relation to island arcs and sea-floor spreading, J. Geophys. Res. 73, 3847-3858.

Stauder, W. (1972). Fault motion and spatially bounded character of earthquakes in Amchitka Pass and the Delarof Islands, J. Geophys. Res. 77, 2072-2080.

Stoiber, R.E. and M.J. Carr (1973). Quaternary volcanic and tectonic segmentation of Central America, Bull. Volc. 37, 304-325.

Swift, S.A. and M.J. Carr (1974). The segmented nature of the Chilean seismic zone, Phys. Earth Planet. Inter. 9, 183-191.

Thrasher, G.P. (1977). Median valley crustal structure and sea floor spreading of the Gorda ridge, 42°N latitude, M.S. Thesis, Oregon State University.

Thrasher, G.P. and S.H. Johnson (1976). Velocity structure of the Gorda ridge near 42°N (abstract), Eos, Trans. Am. Geophys. Union 57, 962.

Tobin, D.G. and L.R. Sykes (1968). Seismicity and tectonics of the northeast Pacific Ocean, J. Geophys. Res. 73, 3821-3845.

Veith, K.F. (1974). The relationship of island arc seismicity to plate tectonics, Ph.D. dissertation, Southern Methodist University.

Vine, F.J. (1963). Magnetic anomalies associated with mid-ocean ridges, in, Phinney, R.H., editor, The History of the Earth's Crust, A Symposium, Princton Univ. Press, Princeton, New Jersy, 73-89.

Vine, F.J. and D.H. Matthews (1963). Magnetic anomalies over oceanic ridges, Nature 199, 947-949.

Von Herzen, R.P. (1964). Ocean floor heat-flow measurements west of the United States and Baja California, Marine Geology 1, 225-239.

Wilson, J.T. (1965). Transform faults, oceanic ridges, and magnetic anomalies southwest of Vancouver Island, Science 150, 482-485.